Faculdade de Engenharia da Universidade do Porto

Drug Delivery Systems for Bone Regeneration

Joana Vicente Nave

MASTER THESIS

INTEGRATED MASTERS IN BIOENGINEERING

Supervisor: Inês Alencastre (PhD)
Co-Supervisor: Ana Paula Pêgo (PhD)

September 2015

RESUMO

A remodelação óssea é regulada por um equilíbrio entre as actividades osteoblástica e osteoclástica. No entanto, em condições clínicas complexas, como sejam as fracturas críticas, a regeneração óssea fica comprometida, sendo requerido um auxílio externo. Deste modo, novos métodos que permitam regular a homeostasia do osso têm sido estudados.

O Neuropéptido Y (NPY) exerce um papel importante na regulação do metabolismo e massa óssea. Estudos realizados no receptor Y1 (um dos 5 receptores do sistema NPY) demonstraram que o seu bloqueio tem um impacto positivo na massa óssea. No entanto, o receptor Y1, que se encontra nas membranas celulares, tem uma ampla distribuição ao longo do organismo, com impacto em outros sistemas fisiológicos para além do osso. Deste modo, o objectivo geral deste projecto consiste na concepção de um sistema de entrega local de fármacos para a entrega no meio extracelular do BIBP3226, um potente e selectivo antagonista do receptor Y1. Com este objectivo, sistemas baseados em partículas e nanofibras foram preparados e optimizados.

Estudos revelaram que para tamanhos abaixo de 200 nm e acima de 500 nm, as partículas têm tendência a ser internalizadas por, respectivamente, células não-fagocíticas e fagocíticas, limitando assim a pretendida distribuição extracelular do fármaco. Deste modo, através da aplicação dos métodos de Salting-out e Nanoprecipitação, foram preparadas partículas de Poli(ácido lático-co-ácido glicólico) com tamanhos compreendidos entre 100 e 1000 nm, de modo a testar a hipótese formulada sobre a internalização em células osteoclásticas derivadas da medula óssea. Resultados mostraram que se uma célula estiver capacitada de realizar fagocitose, ela irá internalizar partículas com tamanhos acima de 500 nm numa escala superior quando comparado a partículas de tamanhos inferiores a 500 nm. Em adição, foi ainda notável que células com mais de 8 núcleos, internalizam menos que células com 2 ou 3 núcleos, levando a concluir que à medida que a célula é mais matura em relação ao fenótipo osteoclástico, menor é a sua capacidade de internalizar partículas. Num estudo realizado em paralelo, os volumes utilizados no método de Salting-out foram variados. Os resultados desta variação mostraram diferenças significativas na eficiência de encapsulação das partículas, mas não para nos seus tamanhos.

Relativamente às nanofibras, estas foram preparadas por Electrospinning, usando Policaprolactona. Estes sistemas têm não só a capacidade de realizar uma entrega de fármacos eficiente, como também fornecem suporte como scaffold. Diferentes formulações, no que diz respeito à concentração de polímero e tipo de solvente orgânico, foram testadas. No entanto, devido à degradação do polímero, o procedimento não foi optimizado. Deste modo, novas experiências neste tópico devem ser realizadas.

ABSTRACT

Bone remodeling is tight regulated by an equilibrium between the osteoblastic and osteoclastic activity. However, in complex clinical conditions, such as critical fractures, bone regeneration is impaired and external help is required. Therefore, new methods of controlling bone homeostasis have been studied.

Neuropeptide Y (NPY) was found to have an important role in the regulation of bone metabolism and mass. In effect, studies have shown that blocking Y1 receptor (one of the 5 receptors from the NPY system) has a positive impact in bone mass. However, Y1 receptor, which is located at cell membranes, has a wide distribution throughout the body, with impact in other physiological systems. Therefore, the overall goal of the project is the design of a local drug delivery system for the extracellular delivery of BIBP3226, a potent and selective Y1 antagonist. Therefore, particles and nanofibers based systems were optimized and prepared.

Studies have revealed that for sizes below 200 nm and above 500 nm, particles have a tendency to be internalized by non-phagocytic and phagocytic cells, respectively, thereby hampering the aimed extracellular delivery. Therefore, the Salting-out and Nanoprecipitation methods were applied in the preparation of Poly(lactide-co-glycolide) particles with sizes ranging from 100 nm to 1000 nm, in order to test the abovementioned internalization hypothesis in Bone Marrow derived Osteoclast Lineage cells. Results have shown that if a cell is capable of internalize particles with sizes above 500 nm (i.e., if a cell is capable of performing phagocytosis), it will internalize them in a larger scale than particles with sizes below 500 nm, as Large particles were, in a general way, more internalized than the other differently sized particles. Furthermore it was noticeable a tendency for a lower internalization in cells with more than 8 nuclei, leading to the conclusion that as the cell is more mature towards osteoclasts phenotype, it has less capacity to internalize particles. In a parallel study, the volumes used in the preparation of particles by Salting-out were varied in order to assess if this variability had influence on the particles' size and drug loading efficiency. The obtained results have shown significant differences in loading, but not in size.

Regarding nanofibers, these were prepared by Electrospinning, using Polycaprolactone. Nanofibers have not only the capacity of performing an efficient drug delivery, but they can also provide support as a scaffold. Different formulations regarding polymer concentration and the organic solvent were tested. However, due to the polymers' degradation, this procedure could not be optimized. Therefore, further experiments on this topic should be performed.

AKNOWLEDGMENTS

Em primeiro lugar, quero agradecer à minha orientadora, Inês Alencastre, por todo o apoio, carinho e pela paciente orientação que me disponibilizou ao longo deste percurso, exigindo sempre mais e melhor. Estou também verdadeiramente grata à minha co-orientadora, Ana Paula Pêgo, por todos os conselhos, apoio incondicional e ensinamentos que contribuíram para o meu crescimento intelectual e como pessoa. Agradeço ainda a toda a equipa NOG que me acolheu no desenvolver deste projecto: à Meriem Lamghari por toda a motivação e ânimo no trabalho, à Dani e ao Francisco que tanto batalharam comigo para que tudo corresse bem, à Juliana pela simpatia, preocupação e auxílio, à Estrelinha que tantas vezes abdicou do seu tempo para me ensinar e orientar sempre no melhor caminho, com toda a simpatia, carinho e alegria e, porque os últimos são sempre os primeiros, ao Luís Campeão, o meu maior apoio destes meses, a quem um bilião de agradecimentos seria muito pouco. Quero também expressar a minha gratidão a todos os que de uma maneira ou outra ajudaram e disponibilizaram o seu tempo no desenvolvimento deste projecto, em especial à Rute Nunes, à Vicky, à Juliana Dias, à Joana Furtado, à Maria Lazaro e ao João Martins.

Aos meus pais quero agradecer com todo o meu coração por sempre me terem dado do pouco que tinham para eu conseguir alcançar uma vida melhor. Ao meu irmão agradeço pelo companheirismo, amizade e por toda a educação que me deu como segundo pai que sempre foi. Aos meus primos, tios e avó, por toda a amizade, alegria e apoio ao longo desta caminhada, deixo-lhes um brinde ao *Monsieur Conan Correia*!

A todos os grandes (enormes!!) amigos que fiz durante estes 5 anos, agradeço por todo este percurso de jantaradas, risadas e boas (ou más acabadas em boas) histórias. Aos Sal(sich)inhas por todos os dias de trabalho que se tornaram *hilários*. Ao conjunto das 8 Bacocas mais os Faustos, de quem guardo as melhores recordações (mas decerto que o futuro ainda nos guarda muitas mais!). To Sarah, Iza, Ula and Laura, the funniest and happiest girls I've ever met! À minha Clarinha e Bruna, por todas as vezes em que pensaram no meu colesterol e ainda assim acharam por bem fazer-me massa com atum para jantar, por todas as conversas incluídas nos capítulos "*um dia, quando formos velhinhas, vamo-nos lembrar destas conversas de sofá*" e por todo o apoio e amizade incondicionais, 23 horas por dia (na outra hora eu estava a lavar a louça… sozinha). Ao António, por sempre acreditares no meu sucesso, por toda a paciência, amizade e carinho que partilhámos ao longo deste tempo.

Joana Nave

“I have not failed. I’ve just found 10,000 ways that won’t work.”

Thomas A. Edison

CONTENTS

LIST OF SYMBOLS AND ABBREVIATIONS

α – MEM	Minimum Essential Medium Eagle – Alpha Modification
ACN	Acetonitrile
AR	Aspect-Ratio
BMC	Bone Marrow derived Osteoclast Lineage Cells
BMPs	Bone Morphonegenetic Proteins
BSA	Bovine Serum Albumin
C	Conditional Knockout
d	Diameter
DAPI	4′,6-Diamidino-2-phenylindole dihydrochloride
DCM	Dichloromethane
DLS	Dynamic Light Scattering
DMF	N,N- Dimethylformamide
DMSO	Dimethyl Sulfoxide
ECM	Extracellular Matrix
EDTA	Ethylenediamine Tetraacetic Acid
FBS	Fetal Bovine Serum
G	Germline Knockout
h	Height
Hyp	Hypothalamus Knockout
M-CSF	Macrophage Colony-Stimulating Factor
$MgCl_2.6H_2O$	Magnesium Chloride Hexahydrate
mPEG-PTMC	Monoethoxy poly(ethylene glycol)-poly(trimethylene carbonate)
MPS	Mononuclear Phagocyte System
MSCs	Mesenchymal Stem Cells
MSNs	Mesoporous Silica Nanoparticles
NPY	Neuropeptide Y
PBS	Phosphate Buffered Saline
PCL	Polycaprolactone
PDI	Polydispersity Index
PEG	Polyethylene Glycol
PFA	Paraformaldehyde
PLA	Poly Lactid Acid
PGA	Poly Glycolic Acid
PLGA	Poly(lactide-co-glycolide)

P/S	Penicillin/Streptomycin
PTMC	Poly(trimethylene carbonate)
PVA	Poly(vinyl alcohol)
PVN	Paraventricular Nucleus
RANKL	Receptor Activator of Nuclear Factor Kappa-B Ligand
rhBMP-2	Recombinant Human Morphogenetic Protein-2
rhBMP-7	Recombinant Human Bone Morphogenetic Protein-7
RNA	Ribonucleic Acid
Rpm	Rotations per Minute
RT	Room Temperature
RT-PCR	Real Time – Polymerase Chain Reaction
TRAP	Tartrate Resistant Acid Phosphatase
TGF-ß	Transforming Growth Factor ß
THF	Tetrahydrofuran
Wt	Weight
Wt/vol	Weight /Volume

LIST OF FIGURES

LIST OF TABLES

CHAPTER 1

Literature Review

1.1. BONE

1.1.1. General Considerations

Bone is a complex and dynamic tissue with the ability to adapt to its functional demands and repair itself [1]. It is considered to be a connective tissue that functionally interacts with several other organs and tissues [2]. This tissue has an important role in mechanical (it supports the whole body and allows locomotion), protective (it shields vital organs and bone marrow) and metabolic (it acts in the regulation of calcium and phosphate homeostasis) functions [2]. In addition, bone is responsible for the storage of minerals and production of blood cells [3].

In terms of classification, bones can be divided into flat, which corresponds to flat, slender and usually curved bones (e.g. skull), long, which are classified as being longer than wider (e.g. femur), and short or cuboid, which are bones that are nearly as wide and thick as they are long (e.g. carpus) [3, 4].

Bone is essentially made up of cells, extracellular matrix, which is mineralized, water and lipids. Regarding the cellular component, bone is formed by four different cellular interveners: the osteoblasts, with osteogenic functions, the osteocytes, that play a role as mechanosensors in bone remodeling, the bone-lining cells, that cover the bones' surface, and the osteoclasts, with resorption functions [2, 5]. More details about the bone cells will be described in the next section. In what concerns the bone matrix, it is composed by 35% of organic components (mainly formed by fibers of collagen and proteoglicans) and 65% of inorganic component (mainly formed by hydroxyapatite) [2, 3]. Collagen is responsible for the flexible resistance, while the mineral components confer compression resistance, which allows the weight support [3].

Structurally, it can be identified two types of bone: cancellous or trabecular and cortical or compact bone (Figure 1-A). Cancellous bone is the most active bone part in terms of growth, calcium homeostasis and hematopoiesis [4]. It is constituted by interconnected bone

plates nominated trabeculae, between which there is free space that is filled with bone marrow and vessels. The trabeculae are constituted by several lamellae, being the osteocytes placed between them. As, usually, blood vessels cannot cross the trabeculae, the osteocytes can only reach nutrients from the canaliculi, which are the channels that associate the osteocytes in bone. Regarding the trabeculae surface, it is constituted by a cell layer, which is mainly composed by osteoblasts and few osteoclasts [3]. Its supportive functions occur mainly in locations where compression type of loading is predominant (e.g. in vertebral bodies) [4]. Cortical bone (Figure 1-B) is stronger, more static, thicker and with less free space than the cancellous one [3, 4]. The osteocytes and lamellae present in this type of bone are positioned around the blood vessels, which penetrate the bone mass. In fact, in cortical bone, there are two main channels where blood vessels penetrate: the channels parallel to the bone axis, which are called Havers or central channels, and the channels perpendicular to the bigger bone axis, which are called Volkmann or perforating channels. Furthermore, it can also be found in cortical bone the osteon or Havers system, which is constituted by a central channel and its content (which includes blood vessels, nerves and loose connective tissue), concentric lamellae and osteocytes. In fact, it can be distinguished three different types of lamellae present in cortical bone: the concentric lamellae, previously referred as being part of the osteon, which are concentric circular layers of bone matrix that round a common center (center channel); the circumferential lamellae, which are considered to be flat plates that form the external surface of cortical bone; and the interstitial lamellae, which are present between the osteons and consist of remaining of concentric or circumferential lamellae [3]. The main locations of cortical bone include the shafts of long bones and peripheral lining of flat bones [4].

Microscopically, it can also be distinguished two types of bone, accordingly to their collagen fibers organization: the woven and the lamellar bone. In the woven bone the collagen fibers are randomly organized, in different directions. It is present in newborns and in places where fast bone formation occurs (e.g. after a fracture). The lamellar is considered to be the mature bone that organizes itself in thin layers of lamellae. In this case, the collagen fibers of each lamella are organized parallel to one another and angled to the collagen fibers present in the adjacent lamellae. The osteocytes are present in the interior of the gaps, between the lamellae layers [3, 4]. After the formation of woven bone, usually it is organized to become lamellar bone, in a process named remodeling [4]. Figure 2 schematizes the different types of bone at different structural levels, including the cellular level.

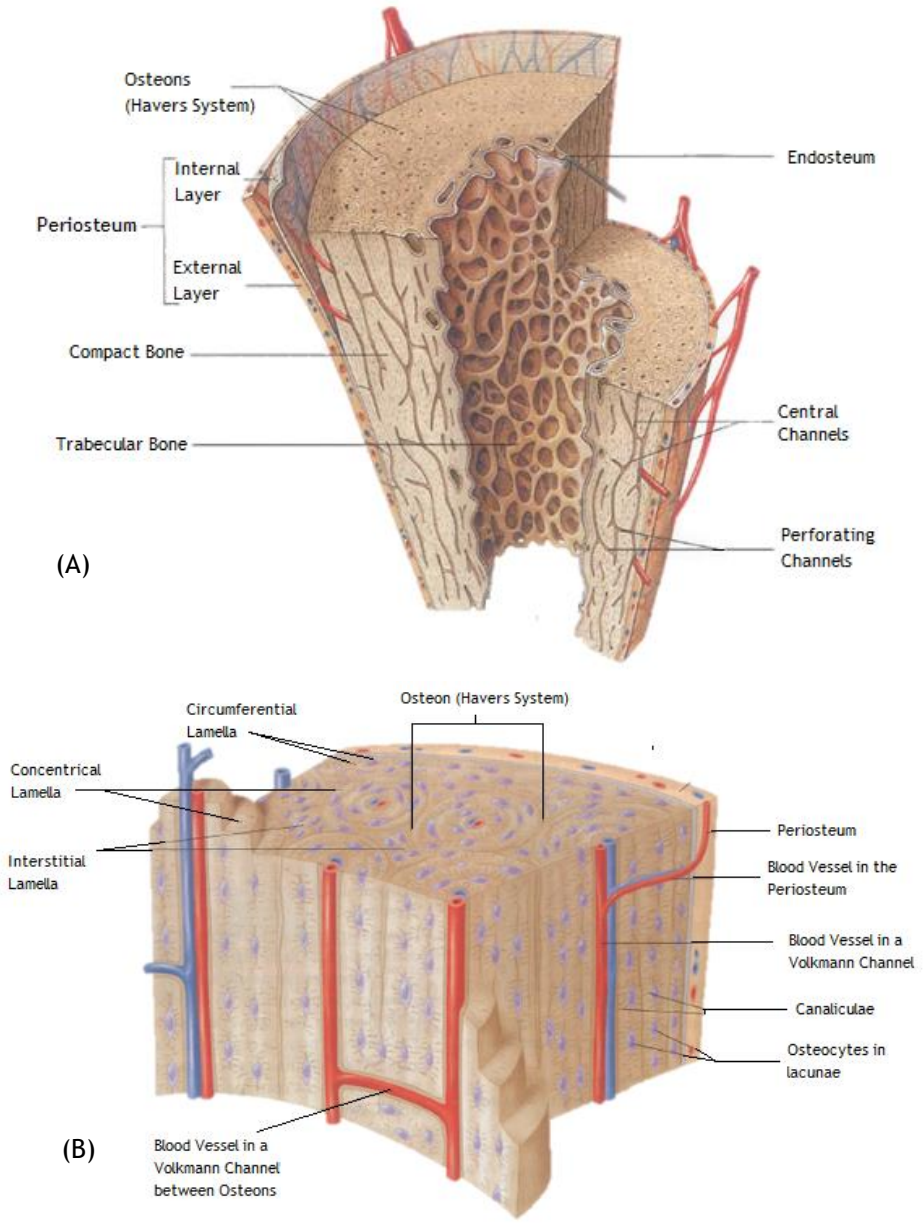

Figure 1. Schematic view of human long (A) and cortical (B) bone. Adapted from [3].

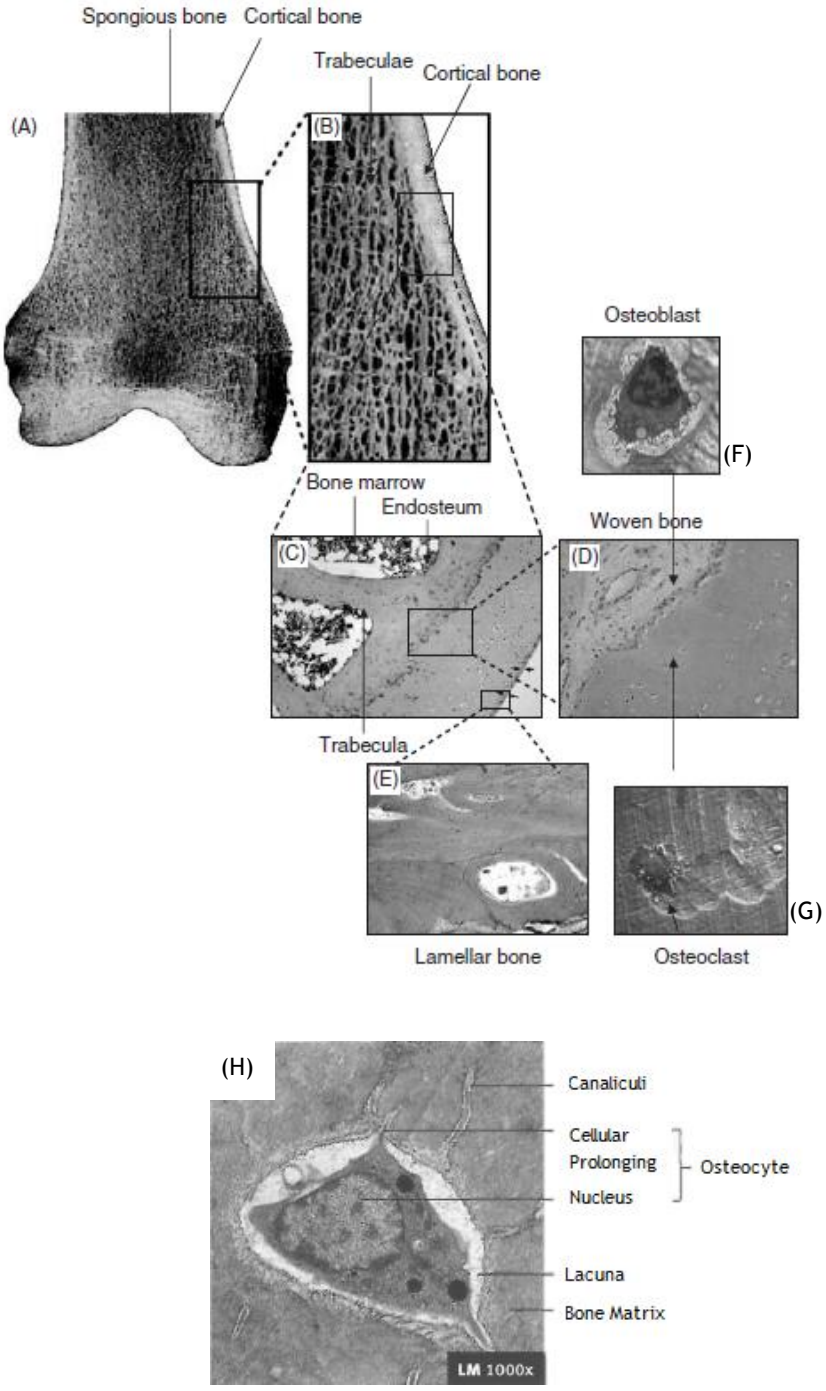

Figure 2. Overview of the different levels on bone structure. (A) Macroscopic aspect of a right femur, with special emphasis on the cortical and spongeous (trabecular) bones. (B) Cortical and the inner spongeous bone in detail, showing the trabeculae that compose the latter referred type of bone. (C) Single trabeculae with bone marrow cavities lined with endosteum on each side. (D) Woven type of bone. (E) Lamellar type of bone. (F) An example of osteoblast from woven bone. (G) An example of osteoclast from woven bone. (H) An example of an osteocyte and surrounding structures. Adapted from [3, 4].

1.1.2. Formation and Remodeling

Bone is continuously being renewed trough a dynamic balance between bone resorption and formation. This constitutes the central basis for the maintenance of normal bone mass and architecture and calcium homeostasis, which is mediated essentially by the osteoclasts (responsible for bone resorption) and osteoblasts (in charge of bone formation) [6].

The bone cells mentioned in the previous section are divided into two main groups: osteoclasts and the osteoblastic family (which includes osteoblasts, osteocytes and bone lining cells) [6].

Osteoblasts derive from mesenchymal stem cells. An example of this type of cell is shown on Figure 2-(F). Osteoblasts have important functions in bone formation, as they are responsible for the deposition of the uncalcified bone matrix (named osteoid), and subsequent mineralization. This mineralization is reached in two steps: firstly, hydroxyapatite crystals are formed within the matrix vesicles; secondly, these mineral crystals are elongated into the extracellular space, filling gaps between collagen fibrils [2]. Moreover, another important function attributed to osteoblasts is the regulation of osteoclast differentiation, as osteoblasts produce important cytokines for this process [2]. At the end of the bone formation phase, osteoblasts have different fates: they can be subjected to apoptosis, become inactive osteoblasts or bone lining cells, or be trapped in the bone matrix as osteocytes [2]. Regarding the bone lining cells, they form a thin continuous layer that covers all bones' surfaces, enabling a controlled movement of ions between the body and the bone. It is considered that the layer of cells located outside the bone is named *periosteum* (this term often includes the collagenous sheet that covers the outer surface); the cells' layer placed on the inside of the bone, it is termed as *endosteum* (Figure 1-(A)) [5]. In what concerns the osteocytes (Figure 2-(H)), they correspond to the cells present in the body of the bone [5]. Although it is possible for them to produce essential components to maintain the bone matrix, compared to the osteoblasts, osteocytes are relatively inactive [3]. Osteocytes are trapped in the hard bone tissue, occupying free spaces called lacunae and connecting with neighboring osteocytes and bone lining cells through cellular prolongations in the canaliculi [3, 5]. Gases and nutrients can circulate through a small quantity of liquid that surrounds cells in the lacunae and canaliculi or by moving from cell to cell, through the gap junctions that join the cellular prolongations [3]. Osteocytes have different functions, from which can be highlighted their role as mechanosensors (they perceive mechanical strain variations and translate it into biochemical signals that will affect bone formation and/or resorption), the regulation of phosphate homeostasis and mineralization, and, in early studies, it was also suggested that osteocytes have the ability to regulate calcium homeostasis [2].

Osteoclasts are big and multinucleated cells that derive from the monocyte-macrophage line. An exemplificative image of these cells is represented on Figure 2-(G). Osteoclasts are responsible for bone resorption or destruction, which is conducted through two different

processes: the acidification to dissolve the inorganic matrix and the secretion of proteolytic enzymes that digest the organic compounds of the bone [2, 3, 5]. The first step occurs when the cellular membrane contacts with the bone matrix, leading to the formation of several projections that will give rise to a ruffled border. Hydrogen ions are pumped through this border, producing an acidic medium that decalcifies the bone matrix. In the second phase, osteoclasts release enzymes that digest the matrix protein components. Some of the products that result from this procedure are conducted to the osteoclast interior through an endocytosis process. Besides this procedure, osteoblasts can also interfere in the resorption process by degrading the non-mineralized organic matrix part. This step performed by osteoblasts allows the direct contact between the osteoclasts and the mineralized bone matrix, enabling a better degradation process [3].

Bone cells mediate not only the formation, but also the bone remodeling. This process occurs in order to substitute the old bone by a new one. Therefore, osteoclasts remove the old bone through resorption processes, and later the osteoblasts deposit the new bone. During the remodeling, the woven bone will be substituted by the lamellar one, making it possible to accomplish different functions, including bone growing, changings in bone configuration, development of new osteons, adaptation to mechanical stress, calcium ions regulation and bone repair [3].

Bone repair can be divided in two basic types: primary and secondary bone healing. Primary healing it is rare and corresponds to the attempt of cells in cortical bone to re-establish the disrupted continuity [7]. In the case of secondary bone healing, it has a characteristic sequence of events that include hematoma, inflammation, formation of soft and then hard callus and remodeling [7]. In the case of, for example, a fracture, there is a disruption of the local tissue integrity, interruption of normal vascular function and distortion of the marrow architecture [3, 7]. This usually leads to the formation of a hematoma with sequential release of inflammatory mediators. This response is characterized by the same steps that occur in other injured tissues: increased blood flow, vascular permeability, migration of inflammatory cells and release of cytokines, and activation of the complement cascade [7]. Consequently, there is a formation of a soft callus, which is a cartilaginous callus. Although it is initially avascular, its subsequent replacement with woven bone involves vascular invasion [3, 7]. The hard callus formation is characterized by an active stage of osteogenesis, osteoblastic activity and formation of mineralized bone matrix. During the formation of the hard callus, the soft callus is gradually removed as revascularization occurs [7] and woven bone is formed [3]. These steps are similar to the ones that occur in endochondral and intramembranous bone formation, which are the processes responsible for skeletogenesis [4, 8]. In fact, the formation of the hard callus can be associated to endochondral bone formation, while the intramembranous bone formation is responsible for the formation of compact or more spongeous cancellous bone [4]. The final process in bone repair will correspond to bone remodeling, which was previously described.

In the clinical setting, the most common form of bone regeneration occurs in fracture healing, which is a specific case of bone repair [8]. However, in some cases, like in large bone defects, the normal biological procedure of regeneration is not enough, what leads to the need of an external help.

1.2. NPY SYSTEM IN BONE REMODELING

1.2.1. NPY Y1 Receptor

Neuropeptide Y (NPY) is a 36-amino acid neurotransmitter [9-12]. that was first isolated from pig brain by Tatemoto et al. [13]. NPY is abundantly expressed in several brain regions [9, 10, 12] with the highest expression occurring in the hypothalamic arcuate nucleus [9, 12, 14]. In the periphery, the adrenal medulla is the primary source of circulating NPY but this neuropeptide is also expressed in liver, heart, spleen and endothelial cells of blood vessels [10], as well as on vascular smooth muscle cells, pancreatic cells, periosteum, bone marrow (particularly in megakaryocytes) [15] and in osteoblasts, osteocytes [9, 12, 15], chondrocites [15], and osteoclasts (unpublished data) [9, 12]. It is also present in the sympathetic nervous system, being co-stored and co-released with noradrenaline upon nerve stimulation [9, 10]. In what concerns the function, NPY is known to play major roles in food consumption regulation, blood pressure, anxiolysis induction, memory retention, circadian rhythms and energy homeostasis [1, 11, 16]. Besides all of these, the discovery of NPY-immunoreactive fibers in bone tissue, associated to blood vessels, bone lining and bone marrow cells [17], indicates that NPY has a central role in regulating bone homeostasis, by performing neuroendocrine actions on bone cells [1, 12].

NPY functions are exerted throughout 5 NPY receptors, termed as Y receptors Y1, Y2, Y4, Y5 and Y6 [1, 9, 12, 18]. From these, so far only Y1 and Y2 were found to play a role in the regulation of bone homeostasis (Table I).

Y2 receptors are expressed in several areas of the brain, such as the hypothalamus, hippocampus, amygdala and brain stem [9, 12, 16]. Peripherally, the Y2 receptors are expressed in white and brown adipose tissue, liver, muscle, spleen and intestine, but not in osteoblasts [9, 12]. The definitive evidence that NPY plays a role in the regulation of bone homeostasis was first revealed by Baldock et al. [19] after germline deletion of Y2 receptors in mice [20]. The results obtained from this deletion shown an increase in cancellous bone volume, which was associated with an amplified osteoblastic activity [19]. Likewise, selective deletion of hypothalamic Y2 receptors in mice resulted in an identical increase in trabecular bone volume within 5 weeks [19]. As no changes of circulating hormones were detected during the experiments, the modulation of bone formation was attributed to the hypothalamic Y2 receptors through neural mechanisms. In addition to this, it was observed that whereas in wild type bone marrow stromal cells Y1 expression was detected (but Y2, Y4, Y5 and Y6 expression was absent), in Y2 knockout bone marrow stromal cells it wasn't detected any Y receptors expression [21]. This was further evidence that the resulting observable effects on bone were related to Y2 central mechanisms, which were probably associated to changings in the Y1 receptor, and not by direct mechanisms in bone cells [19, 21].

Table I. Summary of bone phenotypes from mice after deletion of Y receptors. For Y5 and Y6 receptors there aren't reported conclusions.

Gene Deletion	Y1 (G) [18, 21]	Y1 (Hyp) [18]	Y1 (C) [22]	Y2 (G) [19]	Y2 (Hyp) [19]	Y4 [23]	Y2Y4 [23]	Y1Y2 [18]
Cancellous bone volume	↑	↔	↑	↑	↑	↔	↑↑	↑
Cortical bone mass	↑	↔	↑	↑	↑	↔	↓	↑
Osteoblast activity	↑	↔	↑	↑	↑	↔	↑	↑
Osteoclast surface	↑	↔	↑	↔	↔	↔	↑	↔

G – Germline Knockout; C- Conditional Knockout; Hyp – Hypothalamus Knockout;
↑ - Increased; ↔ - Unaltered; ↓ - Decreased.

Regarding Y1 receptors, they have the widest distribution in the brain, being expressed in cerebral cortex, thalamus, amygdala [11, 16] and particularly in the paraventricular nucleus (PVN) of the hypothalamus [9, 12]. Also, Y1 receptors have a broad distribution in peripheral tissues, including colon, pancreas, adipose tissues, kidney adrenal gland, heart, placenta and, regarding the bone, Y1 receptors are so far the only ones found to be expressed in the osteoblastic lineage and bone marrow stromal cells [12, 15]. In order to evaluate how Y1 receptors knockout would directly influence bone homeostasis, Lundberg et al. [21] performed a study using germline Y1 receptor knockout mice and it was concluded that the alteration of the Y1 receptor signaling leads to a modification in bone formation, as the germline deletion of Y1 receptors resulted in greater bone mineral content and bone mineral density. The same results were obtained by Baldock et al. [18], who demonstrated that the resulting greater bone volume in germline Y1 receptor knockout mice was associated with both osteoblastic and osteoclastic activity. In fact, the results showed that, besides bone formation and unlike what happened in the Y2 receptor knockout studies, bone resorption was also altered in germline Y1 knockout mice, with significant greater osteoclast surface. However, when a hypothalamus-specific deletion of Y1 receptors was performed, the achieved results exhibited no alterations in bone volume neither in bone cell activity when compared to the control group. This led to the conclusion that the Y1 receptor regulates bone homeostasis by a peripheral, non-hypothalamic, pathway. Therefore, with this new insight, new studies have been made in order to evaluate the potential of peripheral Y1 receptors knockout as a new therapeutic strategy on bone metabolism. Lee et al. [24] experiment demonstrated that osteoblastic-specific Y1 deletion resulted in elevated osteoblast activity in male mice, increasing cancellous and cortical bone mass. This suggested that Y1 receptors would be a potential target to treat bone associated diseases. In keeping with this, Sousa et al. [22] showed that the oral administration of a Y1 receptor antagonist to wild type mice resulted in increased bone mass, with high

mineral apposition rate in both cortical and cancellous bone of mice. However, besides this, it was observed an increase in bone resorption indices, which was a behavior only observed in germline deletion of Y1 receptors. This result suggested that Y1 receptor blockage would not only lead to elevate bone mass, but could also lead to an adequate bone turnover, thereby possibly avoiding hypocalcaemia and related complications [22].

As previously referred, there is an Y2-dependent inhibition of Y1 expression in osteoblastic lineage cells that suggests the existence of a mechanism where central Y2 signaling moderates tissue homeostasis [18, 21]. Likewise, the osteoblastic effects from Y1 knockout and Y2 knockout were similar. Therefore, there was the hypothesis that these two receptors were linked in the regulation of bone homeostasis [18]. In order to evaluate this supposition, in the same study previously referred, Baldock et al. [18] performed a germline Y1Y2 double knockout. However, the results showed that deletion of both Y1 and Y2 receptors did not result in additive effects on bone mass when compared to Y1 knockout and Y2 knockout mice. Thus, it was concluded that, although Y1 and Y2 appear to share common pathways in the regulation of bone tissue, there are discrete actions of individual Y receptors, with probable central Y2 and peripheral Y1 effects on bone tissue [15, 18].

Therefore, in order to explore the potential of Y1 receptors, several Y1 receptor antagonist strategies have been investigated in Y1 receptor targeting therapies for diseases such as anxiety [25-31], obesity [32-40], epilepsy [41, 42], between several others. Thus, several effective Y1 receptor antagonists are commercially available in order to determine the pharmacological role of Y1 receptors in targeted diseases.

1.2.2. Anti Y1 Receptor Therapeutic Strategies

The Y1 receptor has a great range of peptide and non-peptide antagonists available. These antagonists have been applied in several experiments, with different purposes. In Table II a summary of the available Y1 receptor antagonists, therapeutic applications and obtained results with the respective administration methods is presented.

Table II. Summary of the peptide and non-peptide antagonists for Y1 Receptor and some of the respective studied applications and results.

Antagonists	Target Therapy	Results	Administration Method	References
BIBO3304	Anxiety	• Attenuation of anxiolysis in the feeding tests, but not in the shock-probe ones	Infusion	[31]
		• Inhibition of the anxiolytic effect	Injection	[30]

	Bone Mass	• Dose-dependently increase in bone mass	Oral	[22]
	Depression	• Attenuation of the antidepressant-like effects	Injection, Infusion	[43, 44]
	Inflammatory Response	• Abolition of the pro-inflammatory action	Injection	[45]
	Food Intake	• Inhibition of feeding behavior	Injection, Injection	[39, 40]
	Pain Modulation	• Prevention of the anti-allodynic actions	Injection	[46]
	Post-Traumatic Stress Disorder	• Prevention of the inhibition of fear responses	Infusion	[47]
BIBP3226	Anxiety	• Potentiation of the anxiogenic and depressive effects of Cholecystokinin tetrapeptide • Induction of an anxiogenic-like effect	Injection Injection, Injection, -	[25] [26-28]
	Atherosclerosis	• Increased atherosclerotic lesion areas	Injection	[48]
	Depression	• Attenuation of the antidepressant-like effects	Injection	[43]
	Epilepsy	• Reduction of the number and time of seizures	Infusion	[41]
	Heart Associated Functions	• Dose-dependent inhibition of the increase in blood pressure • No significant change in heart rate • Smaller infarct volume • Inhibition of the vasoconstriction	- , Infusion Injection -, *In vitro*, Infusion, *In vitro*, *In vitro*	[49, 50] [51] [49, 52-55]
	Hypothalamic-Pituitary-Adrenal Regulation	• The increase of plasma corticosterone levels was contradicted	Infusion	[56]

	Microglial Reactivity	• Suppression of the reduction of interleukin-1β and tumor necrosis factor-α protein generation	*In vitro*	[57]
	Food Intake	• Inhibition of food intake	Injection, Injection	[36, 38]
	Renal Function	• No influence in renal functions in ischaemic heart failure rats	Infusion	[50]
	Reproductive Function	• Inhibition of the increase of Gonadotropin-Releasing Hormone-1 mRNA	*In vitro*	[58]
GI264879A	Food Intake	• Decrease in food intake and body weight	Injection	[32]
GR231118	Anxiety	• Decrease in time spent in social interaction (increased anxiolysis)	-	[27]
	Epilepsy	• Reversion of the anticonvulsant effect of intrahippocampal ghrelin	Microinjection	[42]
	Depression	• Increased depression-like behavior	Injection	[59]
	Heart Associated Functions	• Inhibition of both cardiac slowing and decrease in arterial pressure • Increase in ventilation	Injection	[60]
	Food Intake	• Decrease in food intake stimulated by orexin	Injection	[34]
	Vascular Secretory Function of Salivary Glands	• Inhibition of the attenuation of vasodilation • Inhibition of the pressor response	Injection	[61]
H409/22	Anxiety	• Increase the anxiolytic-effect	Injection	[29]
	Colitis	• Attenuation of the clinical manifestation of the disease	Injection	[62]

	Food Intake	• Suppress of food intake	Infusion	[37]
	Heart Associated Functions	• Inhibition of the vasoconstriction	Infusion	[63]
J-104870	Food Intake	• Suppress of food intake	Injection	[35]
J-115814	Food Intake	• Suppress of food intake and body weight	Oral	[64]
LY357897	Food Intake	• Suppress of food intake	Injection	[33]
SR120819A	Food Intake	• Dose-dependent reduction of food intake	Injection	[39]
	Heart Associated Functions	• Attenuation of vasoconstriction on the kidney	-	[65]
	Lipolysis and Leptin Secretion	• Blockage of the antilipolytic efect evoked by hPYY • Prevention of adipocyte leptin secretion	*In vitro*	[66]

(-) Corresponds to administration methods with unknown information.

BIBO 3304 is the abbreviation for N-[[4-(Aminocarponylaminomethyl)-phenyl] methyl]-N2-(diphenylacetyl)-argininamide trifluoroacetate. This non-peptide compound exhibits selective binding to the Y1 receptor subtype, with more than 1000 to 10000-fold lower affinity for human Y2, human and rat Y4 and human and rat Y5 receptors. Likewise In what concerns its properties to inhibit the NPY mediated signals, no agonistic properties were found to BIBO3304. Thus, it is considered that BIBO 3304 is a potent Y1 receptor antagonist [40] and, when compared to BIBP 3226, it has a 10-20 fold higher affinity for both human and rat Y1 receptors [67]. However, this compound isn't available in radiolabelled form [68]. Chemically, it presents a molecular weight of 757.69.

BIBP 3226 corresponds to the short name for R-N2-(Diphenylacetyl)-N-(4-hydroxyphenyl)-methyl argininamide. It corresponds to a non-peptide Y1 receptor antagonist, exhibiting competitive and excellent Y1 receptor selectivity [49, 69], as it doesn't bind to human Y2 receptor subtype nor cross-react to 60 other experimented receptor types and 15 enzyme systems [70]. BIBP3226 doesn't reveal agonistic properties towards Y1 receptors [69, 70] and therefore it is considered to be the first true non-peptide Y1 receptor antagonist, with characteristics that make it a suitable tool to study the role of NPY in pathophysiological

conditions [70]. This compound has shown to be a fully antagonistic for both neural cells and peripheral tissues [71]. Chemically, BIBP3226 is a hydrophobic compound with a molecular weight of 473.57.

Regarding GI264879A, it is an abbreviation for 1-Substituted-4-methylbenzimidazole (413), N-α-[3,3-bis(1-naphthyl)propionyl]-D-arginine N-[(S)-1-benzyl-2-methoxyethyl] amide. It is considered to be a non-selective and weak NPY receptor ligand, with decreasing affinity for Y1 (which is equal for the Y4), Y5 and Y2 receptors. Regarding its behavior towards NPY mediated signals, GI264879A was tested only for the Y1 receptor and it showed antagonistic properties [32].

GR23118, also named GW1229 or 1229U91, is the abbreviated name for Homodimeric Ile-Glu-Pro-Dpr-Tyr-Arg-Leu-Arg-Tyr-CONH2. Although this peptide compound reveals potent Y1 receptor antagonistic properties, it was discovered that GR23118 is also an agonist for Y4 receptors [72]. Regarding the compound chemistry, it has a molecular weight of 2352.77.

In what concerns H409/22, it corresponds to the abbreviation of the (2R)-5-([Amino(imino)methyl]amino)-2-[(2,2-diphenylacetyl)amino]-N-[(1R)-1-(4-hydroxyphenyl)ethyl]-pentanamide compound. H409/22 is considered to be a potent and selective ligand to Y1 receptors, with antagonistic properties and very low affinity for Y2 and Y5 receptors. However, this compound reveals 5 times lower potential than BIBO 3204 [37]. The molecular weight of this non-peptide compound is approximately 487.61.

J-104870 is the abbreviation for 2-[(4-Chlorophenoxy)methyl]benzimidazoles (411), 6-(5-ethyl-1,3-thiazol-2-ylthiomethyl)-2-[3-methoxy-5-(2-propenyloxycarbonylamino) benzylamino] -4-morpholinopyridine. This compound corresponds to a potent and selective antagonist for the Y1 receptor, revealing low affinities for Y2, Y4 and Y5 receptors. Besides this, it is considered that this non-peptide compound has oral bioavailability and brain penetrability [35]. Its molecular weight is approximately 555.72.

In what concerns J115814, it is the abbreviation for (-)-2-[1-(3-chloro-5-isopropyl oxycarbonyl aminophenyl) ethylamino] -6-[2-(5-ethyl-4-methyl-1,3-thiazol-2-yl)ethyl]-4-morpholinopyridine. This compound has a high affinity to Y1 receptors, but low affinity for Y2, Y4 and Y5 receptors, what reveals its potent and selective Y1 receptor antagonistic properties [73].

LY357897 corresponds to the 1-((1-[3-((3s)(3-Piperidyl))-propyl]-2-[(4-chlorophenoxy)-methyl]indol-3-yl]-2-(4-piperidylpiperidyl)ethan-1-one compound. At the time of its discover, it was classified as being the first selective, subnanomolar Y1 antagonist [33], as it doesn't show appreciable binding affinity for Y2, Y4 and Y5 receptors [71].

Regarding SR120819A, it corresponds to the (2R)-N-[(2R)-3-[4-[N'-[[4-(dimethylaminomethyl) cyclohexyl] methyl] carbamimidoyl] phenyl]-1-oxo-1-pyrrolidin-1-ylpropan-2-yl]-2-(naphthalen-2-ylsulfonylamino)-3-phenylpropanamide compound. It is considered to be a non-peptide, orally active and selective Y1 receptor antagonist [74, 75], as it did not reveal affinity for Y2, Y4 or Y5 receptors [71]. SR120819A has a molecular weight of 750.39.

1.3. DRUG DELIVERY SYSTEMS TO BONE

1.3.1. Current Therapeutic Approaches for Bone Regeneration

For situations where normal bone regeneration is impaired or insufficient, there are currently several therapeutic approaches that, when used alone or in combination, aim the enhancement or management of these complex clinical situations [8].

Bone grafting is a common surgical procedure used to enhance bone regeneration [8]. Bone grafting can be defined as being a strategy where bone from somewhere else is applied in the place where it is needed a stimulation of bone formation. There are three possibilities of bone grafting, being the preferable one the autologous bone graft (the used bone is the patient's own, being usually harvested from locations with relative excess of bone, like the pelvis). The other two options of bone grafting correspond to the allogenic bone graft (the harvested bone belongs to other humans) and the xenogenic bone graft (the used bone graft belongs to other animals from other species) [4]. The autologous bone graft is considered to be the gold standard bone grafting material, as it comprises several advantageous properties: osteoinduction (the extracellular matrix contains bone morphogenetic proteins and other growth factors), osteogenesis (the graft contains osteoprogenitor cells that will contribute to bone formation after the graft is vascularized) and osteoconduction (it works as a scaffold that allows the deposition of bone and integration by the surrounding bone) [4, 8, 76]. Besides this, the autologous bone graft is histocompatible and non-immunogenic, reducing the probabilities of immunoreactions and transmission of infections [8]. Likewise, it can be completely resorbed and remodeled, not interfering with physiologic bone adaptation [4]. However, it presents some disadvantages, as for example limited mechanical strength, quantity restrictions, diverse physical injuries that arise from surgical complications and substantial costs [4, 8, 77]. As an alternative to autologous bone graft, allografts and xenografts were also thought as possible options. The allografts are obtained from human cadavers or living donors. This type of graft surpasses the problems of quantity, as allogeneic bone is available in many preparations [8]. However, as they are devitalized and sometimes demineralized, they do not possess any cellular component, what leads to reduced osteogenic and osteoinductive properties and, consequently, to a delay in the regeneration process [4]. Furthermore, this type of grafts is commonly associated to immunogenicity and rejection reactions and cost problems [4, 8, 78]. In what concerns the xenografts, they are obtained from animals of other species. However, several problems associated to ethics and graft rejection are attributed to this type of graft.

As grafts present several disadvantages, bone-graft substitutes have been developed in the field of bone tissue engineering. These substitutes, named scaffolds, are made of natural or

synthetic biomaterials and aim to promote migration, proliferation and differentiation of bone cells [8]. In order to achieve these goals, bone tissue engineering usually combines scaffolds with biologically active factors, which can be cells, proteins or a combination of both. By doing this strategy, osteoconduction, osteoinduction and osteogenesis are reached. Thus, it becomes necessary to define three different components: scaffolds, growth factors and cells [4].

Scaffolds serve as a delivery vehicle for osteoinductive molecules and/or osteogenic cells. It must fill a gap in a bone defect, facilitating, at the same time, the healing process. However, to perform its purposes, scaffolds for bone regeneration must be biocompatible, osteoconductive, porous (the material must have an interconnected porous architecture in order to facilitate the bone growth inside of the material), biodegradable (this characteristic depends on the final aim of the scaffold, but usually, as bone is regenerated, the material must gradually degrade) and intrinsically osteoinductive [4]. Likewise, scaffolds must have good mechanical properties [4, 8]. In what concerns growth factors, they correspond to signaling molecules that influence certain cellular functions as they bind to specific receptors in cell membranes [4]. The most extensively studied molecules are the bone morphonegenetic proteins (BMPs), which correspond to potent osteoinductive factors [4, 8]. Other growth factors have also been used in different strategies, with different functions regarding cell proliferation, chemotaxis and angiogenesis. These include platelet-derived growth factors, transforming growth factor-ß, insulin-like growth factor-1, vascular endothelial growth factor and fibroblast growth factor, among others [8]. Regarding the cellular component, an adequate supply of cells, such as mesenchymal stem cells (MSCs) and osteoprogenitors, is of major importance in bone regeneration strategies. Usually, these cells are obtained from the bone-marrow, which also contains growth factors, in a minimally invasive procedure [8].

Besides the aforementioned strategies, gene therapies are rising as potential procedures to improve bone regeneration. This method involves the transfer of genetic material into the genome of the target cells, in order to promote the expression of bioactive factors for a prolonged time. However, to apply gene therapies, issues of cost, biological safety and efficacy problems must be solved [8].

In some cases, drugs can also improve bone regeneration. An ideal drug for bone regeneration should restrict its pharmacological activity specifically to bone sites, with minimal effects at a systemic level [79]. However, these drugs are usually administrated alone, orally or parenterally. As bone is a peripheral tissue with limited blood supply, during their pathway, drugs are exposed to various phsycochemical and biological factors, which will affect the drugs bioavailabilty and, thus, their efficient delivery to the required sites. In order to overcome this problem, larger drugs doses are administrated, leading to toxicity problems [80, 81]. Other complications may also arise from the fact that some drugs need to be taken for prolonged duration, resulting in problems associated with the patient therapy compliance [81]. Therefore, new agents and efforts should be made in order to develop new strategies that overcome the

abovementioned problems, enabling improvements in drug efficiency. An example of strategy that has been developed is the controlled drug delivery systems, which make use of different materials with different configurations (e.g. microspheres and nanoparticles). These new developed systems, to be considered as a drug carrier, must be non-toxic (i.e. bioinert or biodegradable), biocompatible, able to incorporate a drug physically or chemically and retain it until it reaches a specific target site, where the drug carrier will gradually be degraded and deliver the drug in a controlled way over time [82]. The materials from which drug carriers are made of, will be chosen accordingly to the desired characteristics, which include chemical characteristics (hydrophobicity or hydrophilicity, molecular size, pi, between others), desired delivery rate, drug release mode, target bone/bones, injury size, whether materials degradation is desired, between other parameters, such as carrier size and structure and drug loading [83, 84]. Therefore, through the combination of different parameters and materials, it is possible to develop new ways of drug delivering, enabling improvements in the field of bone regeneration.

Drug delivery systems can be divided into systemic or local drug delivery. The systemic drug delivery systems are less invasive and usually associated to an oral or parenteral administration. However, these systems can provoke some side effects on non-skeletal tissues [85]. Also, the drugs used in this type of delivery systems should have prolonged circulation time, be able to distribute and accumulate on the target tissues and also they should be protected from enzymatic and chemical degradation [86]. Although it is a more invasive procedure, local delivery of drugs has some advantages towards the systemic drug delivery, as the needed drug quantity is reduced, the side effects are lower, drugs can be retained in the specific local for increased periods and it allows a time-controlled deliver. Ideally, this local drug delivery process should deliver the drug through minimally invasive procedures (e.g. injection to the local site) and possess the ability for in situ matrix formation, allowing an accelerated wound healing, ease in the recognition of requirements of irregular shape defects and augmented patients' comfort and compliance [87, 88].

Therefore, several approaches can be studied in order to improve the actual solutions used to bone regeneration, with special attention to the drug delivery systems.

1.3.2. Nanoparticles Drug Delivery Systems

Nanoparticles have become an important area in the drug delivery systems field as they have the ability to deliver a wide range of drugs to different areas of the body for sustained periods of time, while their small size makes them suitable for systemic circulation [89]. Recent advances in synthesis of polymeric materials with enhanced and advantageous characteristics (biocompatibility, controlled biodegradation profile and responsiveness to biologically-relevant stimuli) are leading to the development of new drug delivery systems [90]. These nanocarriers are divided into two categories: nanocapsules (vesicular system with a

polymeric shell and inner core) and nanospheres (polymeric matrices) [84]. Nanocapsules differ from nanospheres in their constitution: nanocapsules are used in a reservoir form, in which a solid material surrounds a core which is liquid or semisolid at room temperature; nanospheres are matrix particles, which means that their entire mass is solid [91]. In both cases, nanoparticles can be loaded with a wide variety of drugs, including hydrophilic and hydrophobic drugs, proteins, vaccine and biological macromolecules [89]. Drugs can be entrapped inside the nanoparticles or adsorbed on their surface. The first option can be performed by an association of the drug and the nanocarrier during the preparation of the nanoparticles; for drugs that are highly susceptible to degradation, the adsorption on the surface of the nanoparticles becomes a more suitable procedure [91].

There are several methods for the preparation of nanoparticles that allow the production of polymeric nanoparticles with different properties that ensure a proper drug delivery and targeting. These methods can be divided in procedures that include two main steps and the ones that include only one main step. The two steps methods comprise the preparation of an emulsified system (first step), followed by the nanoparticles formation (second step). Usually the second step is achieved either by precipitation or gelation of a polymer or polymerization of monomers. The methods that only require one step are based on the precipitation of a polymer in conditions of spontaneous dispersion formation or due to the self-assembly of macromolecules to form nanogels or polyelectrolyte complexes from a polymeric solution [91].

As nanoparticles have the same size range as parts of natural bone, they are considered as potential candidates for local applications as bone-specific carriers [82]. Furthermore, nanoparticles offer other several advantages, including controlled release properties, protection to the compound of interest and possibility of changing the nanoparticles surface for actively targeting them to specific desired tissues [84, 90]. In order to achieve the desired results, as previously mentioned in section 1.3.1, nanoparticles should comprise a set of characteristics: be nontoxic for cells, effectively carry the molecule of interest and exert their actions specifically on the target, therefore reducing the side effects systemically [82].

As also mentioned in the previous section, the main criteria in choosing a material for drug delivery include not only the chemical characteristics of the drug to be delivered, but also bioavailability, biocompatibility, straightforward production and degradation rate, which enables a sustained release of drugs encapsulated in nanoparticles [84]. Therefore, it becomes essential to perform a previous study on the required delivery parameters and available materials and correspondent characteristics.

1.3.2.1. Polycaprolactone, Poly(lactide-co-glycolide) and Monoethoxy poly(ethylene glycol)-poly(trimethylene carbonate) Polymers

Polymers are versatile materials that can be useful in several applications. For example, hydrophilic polymeric nanoparticles can be applied and used for hydrophilic drugs, gene,

oligonucleotides and small interfering RNA; on the other hand, hydrophobic polymers can be used for water-insoluble drugs [90]. Usually, biodegradable polymeric nanoparticles are preferred as they enable controlled/sustained release, subcellular size and biocompatibility with tissues and cells. Furthermore, these compounds are stable in blood, non-toxic, biodegradable, nonthrombogenic, nonimmunogenic, noninflammatory, do not activate neutrophils and avoid reticuloendothelial system [92]. Polycaprolactone (PCL), Poly(lactide-co-glycolide) (PLGA) and Monoethoxy poly(ethylene glycol)-poly(trimethylene carbonate) (mPEG-PTMC) were previously tested in our group in nanoparticles' preparation procedures [93]. Therefore, a revision on these three polymers was performed in order to understand their characteristics and suitability for the proposed theme.

PCL has a hydrophobic nature [90]. In physiological conditions, this polymer degradation occurs by hydrolysis of its ester linkages. PCL receives a special attention for the preparation of long-term implantable devices [92], as it has a degradation rate of 2 to 3 years, low tensile strength and very high elongation ate breakage [94]. It is also considered to be a semi-crystalline polyester with great organic solvent solubility [94]. Regarding its applicability, PCL has been used as a drug carrier in several studies, including anticancer, diabetes (insulin), antifungal (amphotericin B) and clonazepam drugs [92]. However, so far, no PCL nanoparticle delivery system to bone has been reported.

PLGA corresponds to a copolymer of poly lactic acid (PLA) and poly glycolic acid (PGA). PLA is more hydrophobic than PGA and, consequently, lactide rich PLGA copolymers are less hydrophilic, adsorb less water and degrade more slowly. In fact, the 50:50 ratio of PLA/PGA exhibits the highest rate of degradation; for other ratios, as the content of PGA is higher, the degradation rate also augments [95]. After hydrolysis, PLGA produces metabolite monomers (lactic and glycolic acid), which are two monomers with which the body usually deals. However, the acidic nature of this copolymer makes it not suitable for drugs or bioactive molecules. This problem can be overcome by blending the PLGA with other compounds [92]. In what concerns the mechanical strength, swelling behavior, capacity to undergo hydrolysis and biodegradation rate are dependent on the PLGA physical properties (molecular weight, polydispersity index and cristallinity) [95]. This polymer has been widely used to encapsulate and deliver several types of drugs, including anticancer, diabetes (insulin), psychotic, hormonal (estradiol) and tetanus drugs [92]. Regarding specifically the targeting to bone, drug delivery systems based on PLGA micro and nanoparticles have been developed and used as carriers for recombinant human morphogenetic protein-2 (rhBMP-2) [96, 97], recombinant human bone morphogenetic protein-7 (rhBMP-7) [98], transforming growth factor ß (TGF-ß) [99], nafcillin [100], estrogen [101] and dexamethasone [102].

mPEG-PTMC is a diblock copolymer and it is considered to be an amphiphilic compound: the mPEG component constitutes the hydrophilic part, while the PTMC segments are the hydrophobic ones [103, 104]. It degrades very slowly in water and in acidic environments, although in lipase solutions it can be degraded by an enzymatic surface erosion process [104]. In fact, block copolymers containing PEG have been widely used for the development of

controlled delivery systems of drugs. On the other hand, as PTMC doesn't form acidic compounds during its degradation by surface erosion, PTMC-based polymers are also very attractive for the delivery of drugs [104]. The use of this copolymer has been widely described by Zhang et al [104] in several studies regarding the compound characteristics and its use in the preparation on micro and nanoparticles. However, besided the aforementioned studies, mPEG-PTMC has not been described in literature.

1.3.2.2. Nanoparticle Delivery Systems for the Extracellular Space

The cell membrane acts as a barrier or biomembrane that separates the external environment from the inside of the cell. Understanding interactions between particles and this membrane becomes important to predict subsequent biological effects [105].

Internalization of nanoparticles in cells is influenced by several physical and chemical properties of the materials, as well as by the medium characteristics in the moment of the exposure. There are several nanoparticle characteristics that influence their uptake: size, shape and geometry, surface charge and hydrophilicity. The bulk characteristics of the nanoparticle do not play an important role in the particles internalization, as the surface characteristics are the ones that determine the protein corona and therefore biological impact [106].

Several studies have been made with the aim of evaluating how the particles size can influence their uptake by cells. Accordingly to Sylvester et al. [107], nanoparticles of 100 and 200 nm were easily internalized by cells, while particles with 500 nm remained in the extracellular space. Thus, it was concluded that 350 nm would be the ideal size to retain the nanoparticles in the extracellular space. Same results were obtained by Sivaraman and Ramamurthi [108], who also concluded that, although 500 nm size particles are completely excluded by cells, in certain cases they can be phagocyted. These results are in agreement with several others that demonstrate that nonphagocytic cells favor the uptake of smaller particles while larger particles aren't internalized by these same cells [109-114]. However, there isn't agreement in which is the exact size that leads to the exclusion of the particles by nonphagocytic cells [114]. Regarding the phagocytic cells, although some results have shown that there is a particle size-dependent uptake [115], there isn't clear evidences that this procedure is unequivocally related to particle size [106].

Regarding the shape and geometry, Gratton et al. [114] studied the uptake of monodisperse cross-linked PEG hydrogel particles by HeLa cells. The results showed that cylindrical nanoparticles with high-aspect-ratio (diameter (d)=150nm, height (h)=450nm) were internalized faster than the symmetric (aspect-ratio (AR)=1, d=h=200 nm) cylindrical nanoparticles, although they have the same volume. When comparing cylindrical nanoparticles with similar aspect ratio but different diameter (d=100nm vs d=150nm), the results indicated that the particles with smaller diameter were less internalized than the larger ones. The same happened

to cubic particles, as the ones with lower side length were more internalized than the larger particles. Huang et al. [98] obtained the same results with mesoporous silica nanoparticles (MSNs) and A375 human melanoma (A375) cells, as particles with smaller AR had minor interaction with cells. However, these results were contradicted by Chithrani et al. [111], as the reported study showed that lower aspect-ratio led to greater cellular uptake. In order to also evaluate the effect of the particles geometry in phagocytosis, Champion and Mitragotri [116] used polystyrene particles with different geometries (spheres, oblate ellipsoids, prolate ellipsoids, elliptical disks, rectangular discs and UFOs) and studied their internalization by macrophages. All shapes were effective in initiating the phagocytosis process in, at least, one orientation. However, this internalization was dependent on the local particle shape, i.e., by measuring tangent angles, it was possible to analyze that the point of initial contact between the particles and the macrophages dictates if the particles will be phagocytized or if macrophages will spread on particles. Here, the particle volume was also an important parameter, as particles larger than cells led to a non-complete phagocytosis. Therefore, there isn't a common sense on which shapes will give rise to the particles uptake, as it is necessary to consider length, diameter and volume of the particles. Likewise, there aren't any clear evidences of which of these parameters is dominant [106] and, thus, fair conclusions about shape and geometry cannot be taken.

Surface charge has been also studied as an important parameter that regulates the particles uptake. To this parameter, studies are more consensual, as the majority of them concludes that zero surface charged particles have lower cellular uptake when compared to charged particles [117-119]. This may be explained by the negatively charged cell membrane [106].

In what concerns hydrophilicity, performed studies using polyethylene glycol (PEG), revealed that as hydrophilicity increases in particles' surface, the uptake of these particles decreases [111, 112, 113].

Besides the aforementioned factors, functional groups are also an important parameter that influences the particles internalization. These functional groups will modify the surface charge or hydrophilicity. Therefore, the same conclusions as the ones above can be taken accordingly to the specificities of the used functional groups. For a more extensive review about the mentioned parameters, [106] can be consulted.

1.3.3. Nanofibrous Drug Delivery Systems

Biomimetic nanostructures, that allow the production of synthetic analogs of different nano-components of the human body (with a special attention to the extracellular matrix (ECM)), have become of major importance in the study of cell biology, in regenerative medicine and medical device design [120]. From the whole set of nanostructures, nanofibers have deserved particular attention, as they can mimic the filamentary ECM or form a fibrous scaffold with encapsulated drugs. Moreover, they have reduced potential health hazards that are associated with discontinuous use of nanomaterials and nanoparticles [120]. The conventional

mechanical fiber spinning, the melt blowing or the island-in-the-sea methods are some of the described methodologies to produce fibrous structures. However, along with being very expensive methods, they cannot produce fibers with nano-diameters. One technique that can both combine the large scale fabrication of nanofibers and simplicity of the process, is electrospinning [120].

1.3.3.1. Electrospinning Process and Therapeutic Applications

Electrospinning is emerging in the biomedical field, as a technique capable of fabricating fibers with nanometer range diameters, yielding very high surface areas, controlled porous architecture, ease of functionalization for different purposes, a 3D microenvironment and the possibility of encapsulating drugs in the nanofibers [120, 121]. It is briefly described as a type of fiber forming process by means of electrostatic forces that control the production procedure [122]. These forces exist to substitute the conventional mechanical forces that are conventionally used to produce a jet [120, 122]. Therefore, by using electrostatic energy, electrospinning's basic principle is that strong electrical forces can overcome the surface tension ones in the polymer liquid [120, 123], allowing the formation of a jet and, consequently, by solvent evaoporation, of polymeric fibers. In order to perform the electrospinning procedure, some elements are required, including a polymer source, a high voltage supply and a collector, which can be either grounded or supplied with a negative charge to further attract the solution [123]. Figure 3 represents a schematic illustration for the electrospinning process.

Depending on the desired application, several polymers can be used to produce nanofibers, from synthetic to natural polymers as well as from copolymer and polymer mixtures to homopolymers [124]. However, it is considered that in a general manner, polymeric solutions must have the following features: a surface tension low enough to be overcome by the electrical field; a charge density high enough to allow the surface tension to be overcome; a viscosity high enough to ensure sufficient chain entanglement to prevent the jet from collapsing into droplets before the solvent is evaporated [125].

Electrospinning technique has been widely applied in tissue engineering applications, with special attention to cardiovascular, neural, musculoskeletal and stem cell engineering [120]. In fact, the large surface areas associated with nanofibers, as well as the structural similarities between nanofibrous membranes and ECM, make nanofibers well suited to promote cell growth and the formation of three-dimensional cellular colonies [125]. Furthermore, nanofibers can also play an important role as being nanocarriers for drug delivery, as their dimensions and surface properties can be specifically tailored to adjust and control the release of active ingredients [125] as well as these carriers can be very malleable in order to be adapted to different applications. Moreover electrospun mats have the ability to overcome drug loading limitations seen with other drug delivery devices [126]. Considering specifically bone

regeneration, nanofibrous matrices present several advantages. As electrospun nanofibers can mimic the topographic features of the ECM, they provide a large surface for cellular interactions in their fiber network, therefore functioning as both structural cell support as well as reservoir for controlled drug or growth factors release [127]. Moreover, nanofibers are able to fill large bone defects as well as they possess porosity [127] in proportions that may improve bone ingrowth *in vivo* [128]. Therefore, several studies have been applied to bone using electrospun nanofibers. These studies are in majority associated with filling defects in bone by using biodegradable materials that aim to promote cell adhesion. Other approaches aim to combine nanofibers with compounds that promote bone regeneration, turning the nanofibers into drug delivery systems. Several studies have been performed with different polymers in order to study the potential of nanofibrous structures as drug delivery systems to bone. Among others, PCL is one of the most extensively used polymers [129-133], as its low degradation rate makes this polymer a great candidate for long-term implants for drug release. Piskin et al [134] have combined simvastatin with PCL, obtaining good results in enhancing bone defect healing. Yoshimoto et al [135] have also studied the potential of microporous PCL scaffolds, made by electrospun fibers, combined with osteogenic factors. Their results have shown that, after four weeks, the constructs were covered with cellular multilayers, showing the great usability of these PCL scaffolds.

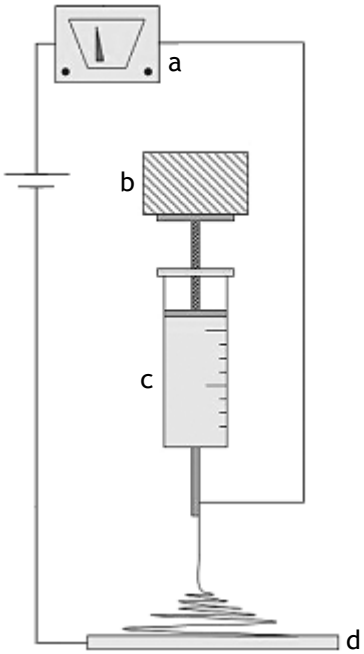

Figure 3. Schematic view of the electrospinning process. (a) high voltage power supply; (b) syringe pump; (c) syringe containing the polymeric source; (d) collector. Scheme adapted from [122, 125].

Therefore, considering all the aforementioned mentioned characteristics, electrospun nanofibers constitute a powerful new source to be explored in the design of solutions for bone regeneration, both by acting as a mechanical support, as well as a delivery system of drugs that may aid in bone formation.

CHAPTER 2

Aim of the Thesis

The NPY Y1 receptor has arisen as a potential regulator in the local control of bone turnover. *In vitro* studies using BIBP3226, a potent Y1 receptor selective antagonist, showed that blocking this receptor has a positive impact in bone mass, thus providing good perspectives for BIBP3226 use as a pharmacological tool for bone regeneration. Still, considering the ubiquitous expression of Y1 receptor in the body and the antagonist intrinsic characteristics (such as its low bioavailability and short half-life), a particle delivery system, that protects the antagonist from clearance and degradation and enables its controlled release to the bone, offers much greater potential as compared to the drug administration alone. Moreover, as nanofibers can both offer support (as a scaffold) for bone regeneration as well as they can work as a delivery system, these nanostructures can also bring advantages in drug delivery for bone regeneration.

Considering the fact that Y1 receptor is located at the cell membrane, a key feature of such system would be drug release at the extracellular space. Therefore, in this work we aim to optimize both a particle and a nanofiber-based systems for the local delivery of BIBP3226 to the extracellular space of bone defects. The specific aims are:

1. Evaluation of the effect of size on particle internalization in bone marrow derived cells. In order to do this, particles with sizes ranging from 100 nm to 200 nm, from 400 nm to 500 nm and from 800 nm to 1000 nm must be prepared.
2. Determination of the cytotoxicity of the differently sized Particles;
3. Design of a nanofibrous delivery system.

CHAPTER 3

Materials and Methods

3.1. Preparation and Characterization of the Polymeric Particles

The particles preparation was performed using three different polymers: PCL (M_n of 80,000 g/mol), which was a kind offer from Diana Leite (INEB) [93], and PLGA with a monomer composition of 55:45 (M_n from 30,000 to 60,000 g/mol) (Sigma-Aldrich, Portugal). Particles were prepared by the Salting-out method, with exception of PLGA that was both used to prepare particles by Salting-out and nanoprecipitation methods. After evaluation of sizes and stability, the following work after particles preparation and characterization was only performed with PLGA.

3.1.1. Particles Preparation

Particles were prepared using both the Nanoprecipitation and the Salting-out methods following protocols adapted from Cheng et al. and Chang et al. [136, 137] and Zhang et al. [138], respectively.

The Salting-out method comprises two steps. Briefly, in a first step, a solution of Tetrahydrofuran (THF) (Sigma-Aldrich, Germany) containing 2.00% (wt/vol) of polymer was emulsified into an aqueous solution containing 60.0% (wt/vol) of Magnesium Chloride Hexahydrate ($MgCl_2.6H_2O$) (Amresco, USA) and variable concentrations of Poly(vinyl alcohol) (PVA) (Sigma-Aldrich, USA), ranging from 0% to 8.00% (wt/vol). This emulsification was performed under mechanical stirring at a speed ranging from 11400 to 29900 rpm (Homogenizer VWR, VDI 12) for 40 seconds. Secondly, after obtaining the oil-in-water emulsion, either an aqueous solution of 0.500% (wt/vol) of PVA (Sigma-Aldrich, USA) or pure water (Synergy Ultrapure Water Systems, Millipore®) was quickly added and stirred for 30 seconds. In order to evaluate the impact of the solutions' volume in particle formation and loading, variable amounts of solutions were used, always maintaining the volumes ratio (Table III). Where nothing is referred in contraire, the volumes used in the Salting-out procedure were the ones referred in Table III as being the Condition 3.

Table III. Volumes of solutions used in the Salting-out method.

Condition	Polymeric Solution in THF (mL)	$MgCl_2.6H_2O$ + PVA Solution (mL)	PVA solution or pure water (mL)
1	1.00	1.82	1.82
2	2.00	3.63	3.63
3	3.00	5.45	5.45

Regarding the nanoprecipitation method, it comprises only one step. Firstly 10 mg of polymer were dissolved in 1.00 mL of Acetonitrile (ACN) (Merck Millipore) or N,N-Dimethylformamide (DMF) (Sigma-Aldrich) and added to 10.0 mL of Milli-Q water (Synergy Ultrapure Water Systems, Millipore®), by means of a 25G needle. This addition was performed under magnetic stirring at a moderate velocity.

Particles loaded with Dexamethasone (Sigma-Aldrich) or Coumarin-6 (Sigma-Aldrich) were prepared accordingly to the previous specifications, except that the polymer was dissolved in a solution of THF containing 1.00%(wt/vol) of Dexamethasone or 0.0300%(wt/vol) of Coumarin-6.

3.1.2. Particles Purification

The particles solutions obtained from the Salting-out method were purified by centrifugation (Eppendorf Centrifuge 5417R) for 30 minutes, at 20ºC. Each polymer had a respective centrifuge force, which are present in the Table IV. After centrifugation the supernatant was removed and the particles were redispersed in an aqueous solution containing 0.125% (wt/vol) of PVA or pure water. The procedure of centrifugation and redispersion of particles was repeated twice.

Table IV. Centrifuge forces used in the purification of the prepared particles with different polymers: PCL, mPEG-PTMC and PLGA.

Polymer	Centrifuge Force ($\times 10^2$ g)
PCL	78
mPEG-PTMC	208
PLGA	52

In what concerns the nanoprecipitation method, the particles were purified by centrifugation or filtration. In the centrifugation option, the method was similar to the one described above for the Salting-out method. However, in this case, the centrifuge force corresponded to 3200 g and the centrifugation time to 20 minutes. The particles were then redispersed in an aqueous solution containing 0.125% (wt/vol) of PVA. The whole procedure was

also repeated twice. Regarding the filtration, the particles solution was filtered using a 1 mL syringe and a 70 μm filter, in a single step.

3.1.3. Particles Freeze-Drying

After the last step of purification, particles were redispersed in a solution containing a ratio of 2:1 (sugar:particle mass ratio) of sucrose. This step aimed to protect the particles against the destabilization induced by the freeze-drying. After this, the particles solutions were frozen at -80ºC and freeze-dried (Bentch top pro) under vacuum for 2 to 3 days.

3.1.4. Particles Characterization

Particles' size and size distribution, which is characterized by the polydispersity index (PDI), were determined by dynamic light scattering (DLS) (Zetasizer Nano, Malvern Instruments) at 25ºC at an angle of 173°. Regarding PDI, it is a dimensionless number that lies between 0 and 1 and indicates the scatter of the size distribution, being 0 the indication of a monodisperse particle suspension. The particles size and PDI were determined accordingly to the ISO13321 (1996) and ISO22412 (2008).

3.1.5. Loading Efficiency of Dexamethasone in the Particles

After Freeze-Drying, Dexamethasone-loaded particles were dissolved into deuterated Dimethyl Sulfoxide (DMSO) (Merck Millipore). Dexamethasone loading of the particles was determined by Proton Nuclear Magnetic Resonance Spectroscopy (^{1}H-NMR) (Bruker Avance III 400 MHz). In order to obtain the results, the integral of the Dexamethasone peaks (1H, δ=7.3-7.28 ppm; 1H, δ=6.23-6.20 ppm; both peaks correspond to –CH groups in the Dexamethasone structure) and the integral of the PLA peak (3H, δ=4.8-4.9 ppm; the peak corresponds to a $-CH_3$ group in the PLA structure) were both calculated. By applying Equation 1 it was possible to determine the maximum possible loading (% wt), while Equation 2 (where *Sum of the integrals of the drug peaks* corresponds to the values obtained by the integration of the above mentioned peaks for the Dexamethasone and *Integral of the polymer peak* corresponds to the the values obtained by the integration of the values obtained for the above mentioned peak for the PLA) allowed the calculation of the theoretical loading (% wt) during the procedure.

$$\text{Theoretical Loading (\% wt)} = \frac{\text{Drug mass}}{\text{Polymer mass}} \times 100$$

(Equation 1)

$$\text{Achieved Loading (\% wt)} = \frac{(\text{Sum of the integrals of the drug peaks})/2}{(Integral\ of\ the\ Polymer\ peak)/3} \times 55$$

(Equation 2)

Therefore, loading efficiency (%) was calculated by the results from the aforementioned Equations.

3.2. Biocompatibility and Internalization assays

3.2.1. Cell Culture

The internalization studies were performed in mice Bone Marrow Cells derived Osteoclast Lineage (which will be abbreviated as BMC). Cells were collected from the femurs and tibias of a C57BL/6 mouse with 12 weeks. Cells were left in culture in Minimum Essential Medium Eagle – Alpha Modification (α-MEM) (Gibco - Life Technologies) supplemented with 10.0% Fetal Bovine Serum (FBS) (Gibco - Life Technologies), 1.00% Penicillin Streptomycin (P/S) (Gibco- Invitrogen) and 30 ng/ml of M-CSF (PeproTech EC). After 3 days of incubation at 37ºC in fully humidified atmosphere of 5% CO_2, the attached cells were harvested with 0.05 M EDTA (Sigma-Aldrich) at a pH 8, seeded in μ-Slide 8 Well Plates (Ibidi) at a density of $1x10^5$ cells/well and cultured in the above described medium supplemented with 100 ng/ml of RANKL (PeproTech EC). The addition of these cytokines aimed the differentiation of the BMC into osteoclasts. Culture medium was replaced at every 3-4 days for up to 7 days.

Following 3 and 7 days of differentiation, cells were incubated with Coumarin-6 loaded particles of three different sizes at a concentration of 0.0400% (wt/vol) and 10.0% Resazurin (as mentioned in more detail in the section 3.2.2). After 3 hours of incubation at 37ºC and 5% CO_2, Resazurin results were assessed and Live/Dead assay and F-actin staining were performed. Controls using cells incubated in the absence of particles and in the presence of 0.000600% (wt/vol) of Coumarin-6 were performed.

3.2.2. Resazurin Assay

Cell metabolic activity was assessed by the Resazurin assay. Therefore, at the time of the addition of the particles, 10.0% (v/v) of Resazurin (Sigma-Aldrich) was added to each well and incubated at 37ºC and 5% of CO_2. Following, 150 μL of the supernatant were transferred, in duplicate, into a black 96-well plate and the fluorescence (λ_{ex} = 530 nm and λ_{em} = 590 nm) was measured using a microplate Fluorometer (Spectra Max GeminiXS Molecular Devices). Blanks for fluorescence emission subtraction were performed with cell culture medium, Coumarin-6 and particles of each size.

3.2.3. Live/Dead Assay

The percentage of viable cells was calculated by the Live/Dead assay. After the 3 hours of incubation with the particles, cells were rinsed twice with Phosphate Buffered Saline (PBS), and incubated with Calcein AM (Molecular Probes – Invitrogen) (1:1000 in warmed PBS 1x) for 20 minutes, at 37ºC, 5% of CO_2. Following, cells were rinsed twice with PBS and incubated with Propidium Iodide (Sigma-Aldrich) (1:500 in warmed PBS 1x) for 5 minutes, at 37ºC, 5% CO_2. Results were assessed with an inverted microscope Leica DMIRE2 (Leica Microsystems, Germany), using the LCS 2.61 (Leica Microsystems, Germany) software.

3.2.4. Immunocytochemistry for F-Actin assay

In order to evaluate cell morphology, an immunocytochemistry for F-Actin assay was performed. After the 3 hours of incubation with the particles, cells were washed twice with PBS, fixed with 4.00% Paraformaldehyde (PFA) (Sigma-Aldrich) for 10 minutes at 4ºC and permeabilized in ice-cold 0.250% (v/v) Triton X-100 (Amersham Biosciences-VWR) (in PBS 1x) for 5 minutes. In order to block non-specific binding, cells were incubated with 1.00% (wt/vol) Bovine Serum Albumin (BSA) (in PBS 1x) for 1 hour. Cells were then stained with Alexa Fluor 594 Phalloidin (Life Technologies) (1:100 in PBS 1x) at room temperature (RT) for 20 minutes in the dark. After rinsing the cells twice with PBS, they were incubated for 5 min at RT with 4′,6-Diamidino-2-phenylindole dihydrochloride (DAPI) (Sigma-Aldrich) (1:1000 in PBS 1x). Samples were analyzed by Inverted Fluorescence Microscopy (Axiovert 200M (Zeiss)) using the Axiovert software.

3.3. Electrospun Fibers

Nanofibers were produced following a protocol adapted from Liliana Pires et al. [139]. In order to test which formulation was better, PCL was used as the polymer and Dichloromethane (DCM) (VWR Chemicals) and N,N-Dimethylformamide (DMF) (Sigma-Aldrich) were the solvents. The previously optimized conditions to perform the experiment were the following: flow rate of 1 mL/hour using a syringe pump (Ugo Basile, Italy); an electric field (Gamma High Voltage source, Ormond Beach, FL, USA) of 1 kV/cm, applied between the tip of the syringe (inner diameter of 0.8 mm) and a flat copper plate (15x15 cm) separated by 14 cm. To achieve this, different formulations of the polymeric solution were used: three different solutions containing a DCM and DMF volume ratio of 1:0, were prepared with a concentration of 10.0%, 13.0% and 15.0% (wt/vol) of PCL; a solution containing a volume ratio of 4:1 was prepared with a concentration of 10.0% (wt/vol) of PCL. All the solutions were tested and the fibers were collected in an aluminum foil for 1 up to 1.5 hours. Images from the produced results were analyzed in an Inverted Fluorescence Microscope Axiovert 200M (Zeiss) and Axiovert software.

3.4. Statistical Analysis

The statistical analyses were performed, where specified, using the IBM SPSS Statistics 20.0 software. Shapiro-Wilk test was applied to assess the normality of the samples. One way ANOVA tests were performed in order to test the homogeneity of the samples, with following Post Hoc (for parametric samples) or Kruskal Wallis followed by Mann Whitney (for non-parametric samples). Results were considered significantly different for samples with $p \leq 0.05$.

CHAPTER 4

Results and Discussion

4.1. Optimization of the Particles Preparation Procedure

The polymeric solution used to prepare particles will strongly affect the structure, properties and application of the particles [89]. As it is intended the delivery of a hydrophobic drug, the initial choice of polymers was centered in hydrophobic and amphiphilic compounds: PCL, PLGA and mPEG-PTMC, available in our laboratory. However, Zhang et al. [138] reported that in the case of mPEG-PTMC the particles size does not vary significantly in spite of large variations in the procedure parameters. This property is associated with the self-stabilizing properties of the mPEG segment. Considering that one of the aims of the present work was to prepare differently sized particles, this polymer was not considered for the study. Therefore, only PCL and PLGA were initially assessed in what concerns their performance during the preparation and purification procedures and, consequently, one of them was chosen has being the more suitable for performing the following experiments.

In addition to the delivery of an hydrophobic drug, it is intended that the delivery occurs in the extracellular space, as the Y1 receptor is transmembranar. Although some studies refer desirable characteristics in particles for an extracellular delivery, there is not a consensus in which are the most suitable ones. As reviewed by Kettler et al. [106] there are some studies referring that non-phagocytic cells will easily uptake smaller particles, usually with a size bellow 200 nm, by endocytosis, while phagocytic cells will uptake the larger ones, usually with a size comprised between 500 nm and 1000 nm, by phagocytosis. Therefore, taking in consideration a heterogeneous cellular population such as the bone marrow, where there is a presence of both phagocytic and non-phagocytic cells, a size between 200 nm and 500 nm would possibly be the most suitable choice. However, to the best of the author's knowledge, none of these studies was performed in bone cells. Therefore, the Salting-out and Nanoprecipitation methods were optimized in order to prepare particles with dimensions ranging from 100 nm to 1 μm: a first group with particles with a size from 100 nm to 200 nm, a second one with sizes ranging from 400 nm to 500 nm and a last one with particles having a diameter comprised between 800 nm and 1000 nm. By obtaining these three differently sized

groups, it would be possible to assess the behavior of the cells when incubated with the particles and verify if the hypothesis that a size between 200 and 500 nm is confirmed.

In an initial phase, Salting-out was the chosen method to prepare particles. The Salting-out method is included on the methods for the preparation of particles that comprise two main steps. The first step corresponds to the preparation of an oil in water emulsion. In order for this to happen, the polymeric solution is emulsified into an aqueous solution containing high concentrations of a salt (in this case, Magnesium Chloride) with strong salting-out effect. The polymer is, at this stage, dissolved in the droplets of the emulsion. The second step of the method corresponds to the particles formation, which occurs by the polymer precipitation. This precipitation is induced by diluting the emulsion with a large excess of water. This dilution will lead to a drop in salt concentration in the continuous phase of the emulsion, inducing the polymer solvent to migrate out of the emulsion droplets and, consequently, forming the particles. The whole procedure is usually aided by mechanical processes (in this case, by homogenization). In order to improve the stability of the final polymeric particles, a stabilizer (in this system, it was used PVA) can also be used [91]. With the aim of obtaining differently sized particles, some parameters on the Salting-out method were varied. With effect, the parameters on this procedure can be easily modified in order to obtain differently sized particles: by augmenting the polymer's concentration and polymer molecular weight, it is possible to obtain larger particles. A reverse situation occurs with the stirring rate and stabilizer concentration, as the increase of these parameters leads to smaller particles. The type of solvent, surfactant and cryoprotectant used for Freeze-Drying are also influencing parameters on the final particles' size results [140]. Therefore, taking into consideration all these factors, variations in both the stirring rate and the stabilizer concentration were performed in order to modulate the particles size and polydispersity index (PDI), which corresponds to an dimensionless number, between 0 and 1, indicating the scatter of the size distribution, being 0 the indication of a monodisperse particle suspension. Both size and PDI were obtained by measurements performed in Zeta-Sizer. However, as it will be discussed hereinafter, as it was not possible to obtain particles with a size below 250 nm by this method, another method was tested: the Nanoprecipitation.

In what concerns Nanoprecipitation, it is constituted by only one step and it has three basic ingredients: the polymer, the polymer solvent (in this case, acetonitrile and N,N-dimethylformamide) and the non-solvent (in this experience it was chosen water) of the polymer. In order to produce the particles, the polymeric solution is added to the non-solvent. The particles form instantaneously, as the polymer solution rapidly diffuse in the non-solvent solution [91] and the polymer chains aggregate forming particles [141]. In what concerns this procedure, the obtained particles can have different sizes by varying the polymer's concentration and molecular weight, the solvent's and surfactant's nature and the phase injection. The presence of additives and active component entrapment may also influence the

obtained sizes [140]. In the performed experiments, only the solvent's type was varied in the Nanoprecipitation procedure. However, as the particles prepared by this procedure were too small, it was also studied the influence of the purification procedure on the obtained particles, as centrifugation could be too powerful for such small particles and, consequently, lead to their aggregation.

In addition to the achievement of differently sized particles, it was performed a parallel study in which the volumes used in the Salting-out method were varied in order to evaluate the influence of this variation in both particles' size and drug loading. Results are shown hereinafter.

4.1.1. Polymer Effect

Both PCL and PLGA particles were prepared equally by the Salting-out method: 5.00% (wt/vol) of PVA in the first step and 0.500% (wt/vol) of PVA in the second one, followed by purification by centrifugation with 0.125% (wt/vol) of PVA.

During the procedure of particles preparation, the two polymers had a similar behavior, as they equally originated a suspension of particles, which was noticeable for the suspensions' milky appearance. Moreover, the characterization of the particles regarding their size and PDI (Figure 4) reveals the presence of particles with a narrow distribution of sizes, as the PDI is low for all the prepared particles.

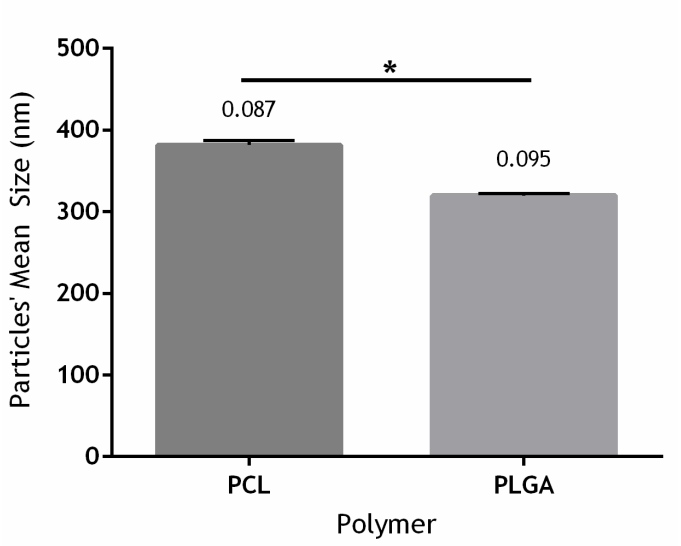

Figure 4. Mean Size of the particles prepared with PCL and PLGA. The particles were prepared by the Salting-out method, comprising solutions with 5.00% (wt/vol) of PVA in the first step and 0.500% of PVA in the second one. The purification of these particles was performed with a solution of 0.125% (wt/vol) of PVA. The homogenization velocity was $2990x10^1$ rpm for all the different polymeric particles. The size and PDI from the particles, both obtained by DLS, were measured right after purification. Results are presented as Average ± Standard Deviation (n=3, i.e., for each polymer it was prepared one batch and for each batch 3 measurements were performed). At the top of each bar is represented the mean PDI values for each group. * Particles' size was significantly different between the signaled conditions, considering $p \leq 0.05$.

It is noticeable that the particles' size differs from one polymer to another, which is associated with polymers molecular weight: the higher the molecular weight, the larger the particles are [140, 142]. This is in agreement to the obtained results as PLGA has a lower molecular weight than PCL. The hypothesis behind this assumption is that polymers with higher molecular weight will lead to a more viscous polymeric solution [142], thereby affecting the stirring process. In turn, this will conduce to larger emulsion droplets, resulting in larger particles. After preparation, particles were purified by centrifugation in order to remove impurities and excess reagents.

If in one hand, the two polymers had a similar performance during the preparation phase, the same has not happened during the purification procedure. It was expected that, after centrifugation, the particles in suspension formed a pellet, which allowed to discard the supernatant followed by resuspension of the particles in 0.125% (wt/vol) of PVA in water and new centrifugation. However, for PCL, this did not occur and the polymeric particles formed a film at the liquid surface, leading to a loss of particles mass, as the task of discarding the supernatant was hampered. It is hypothesized that PCL has degraded with the time, therefore leading to this problem.

In what concerns particles formed with PLGA, they formed a pellet, as well as they were easily redispersed after centrifugation. Therefore, this polymer revealed a more suitable behavior for the intended following work, being, from the three initially proposed polymers, the selected one to proceed this project.

4.1.2. Effect of Volumes' Variations on both Particles' Size and Drug Loading Efficiency

The Salting-out method was optimized by Zhang et al. [138] for a volume of polymeric solution of 5.5 mL. This protocol was adapted by Diana Leite [93] for a volume of polymeric solution of 3 mL, adjusting all the other solutions' volumes so as to maintain the same ratio between them. However, as BIBP3226 is a very expensive reagent, in order to spend less reagents and drug per batch, it was evaluated if the variance of the volumes would affect both the particles' size and drug loading efficiency. Therefore, PLGA particles were prepared by the Salting-out method, accordingly to the optimization performed by Diana Leite [93]: 2.00% (wt/vol) of PVA in the first step and 0.500% (wt/vol) of PVA in the second one, followed by purification by centrifugation with 0.125% (wt/vol) of PVA; the polymer concentration corresponded to 2.00% (wt/vol) and the drug concentration to 1.00% (wt/vol). Three different trials were performed as explained in the Section 3.1.1 (Condition 1 was prepared with the lowest volumes, Condition 2 correspond to the particles prepared with intermediate volumes and the largest volumes were addressed in Condition 3).

The obtained results (Figure 5) show that, although not statistically different, Condition 1 had a larger size when compared to conditions 2 and 3. The volumes used in Condition 1 did not

cover completely the homogenizer tip, which may have influenced the homogenization efficiency and led to the obtained results. However, as results were not statistically different, this circumstance did not influenced significantly the particles' size.

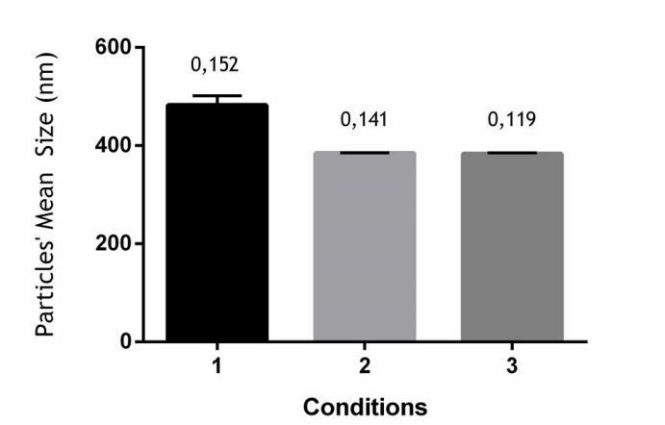

Figure 5. Mean size of the particles prepared with different volumes. Volume from Condition 1 corresponds to the particles prepared with 1 mL of polymeric solution, Volume from Condition 2 regards the particles prepared with 2 mL of polymeric solution and the Volume from Condition 3 comprises the particles prepared with 3 mL of polymeric solution. All the volumes for the used solutions in the preparation procedure are specified in the Table III, Section 3.1.1. The particles were prepared by the Salting-out method, comprising solutions with 1.00% (wt/vol) of Dexamethasone, 2.00% (wt/vol) of PVA in the first step and 0.500% of PVA in the second one. Purification was performed with a solution of 0.125% (wt/vol) of PVA. The homogenization velocity was $2990x10^{1}$ rpm. The size and PDI from the particles, both obtained by DLS, were measured after purification. Results are presented as Average ± Standard Deviation (n=3, i.e., for each batch 3 measurements were performed). At the top of each bar is represented the mean PDI values for each group.

Drug entrapment efficiency is usually associated to a set of parameters related with the particles preparation method. By increasing the polymer concentration, the organic phase viscosity is increased, leading to a higher diffusional resistance to drug molecules from the organic phase to the aqueous phase and, consequently, to the entrapment of more drug in the polymer particles. On the other hand, by increasing the aqueous phase volume, larger particles, which are reported as having higher drug contents, are formed. By increasing the initial drug content, the drug incorporation process operates until its maximum efficiency, determined by the drug miscibility in the polymer at the given conditions, and then it reaches a plateau. Therefore, drug and polymer's characteristics must be studied in order to better understand their interaction. Finally, by decreasing the stabilizer concentration, the drug content in the particles increases, which is mainly associated with the augmentation in the particles size [143]. In the case of the purification phase, other parameters can be modified such as decreasing the volume of the used purifying aqueous solution. By decreasing this volume, the solutions' saturation will be reached more quickly, forcing the drug to be adsorbed at the particles surface. With this in mind, drug loading efficiency was evaluated by ^{1}H-NMR for the 3 conditions prepared with different volumes (Table V).

Table V. Drug loading efficiency of the prepared Dexamethasone loaded PLGA particles with different volumes. Condition 1 corresponds to the particles prepared with 1 mL of polymeric solution, Condition 2 regards the particles prepared with 2 mL of polymeric solution and the Condition 3 comprises the particles prepared with 3 mL of polymeric solution. All the volumes for the other used solutions in the preparation procedure are specified in the Table III, Section 3.1.1.. The particles were prepared by the Salting-out method, comprising solutions with 1.00% (wt/vol) of Dexamethasone, 2.00% (wt/vol) of PVA in the first step and 0.500% of PVA in the second one. Purification was performed with a solution of 0.125% (wt/vol) of PVA. The homogenization velocity was $2990x10^{1}$ rpm. Results were obtained, after Freeze-Drying, by ^{1}H-NMR and using Equations 1 and 2, being the Loading Efficiency calculated by considering the theoretical loading as being 100% (n=1).

Condition	Loading (% wt.)		Loading Efficiency (%)
	Theoretical	Obtained	
1	50.00	5.45	10.9
2		1.18	2.36
3		1.43	2.86

As it is observable, Condition 1 has the highest drug loading efficiency. This may be associated to the larger particles' size obtained for this condition (although sizes were not statistically different, Condition 1 had a larger size). However, the result here obtained for Condition 1 is similar to the one obtained by Diana Leite [93], who has prepared Dexamethasone loaded PLGA particles, using a volume for the polymeric solution of 3 mL (i.e., used the same conditions as the ones defined in this project for condition 3). Therefore, these results suggest that the differences in volume may not affect the loading and the reason beyond the differences here obtained are associated with problems occurred during the preparation procedure. For confirmation, more independent batches should be further prepared and characterized in regards to their size and loading efficiency.

4.1.3. Particles' Size Optimization

As previously referred, it was initially stipulated that sizes should be optimized for three different ranges of particles' sizes, between 100 nm and 1 μm: Small Particles should have a size between 100 nm and 200 nm, Medium Particles should range between 400 nm and 500 nm and Large Particles should vary between 800 nm and 1000 nm. In order to obtain these particles, the Salting-out method was initially chosen to prepare the particles. Therefore, stirring rate and surfactant concentration were modified during the procedure with the intention of modifying the particles size.

Accordingly to different studies [138, 144, 145], an increase in the stirring rate results in a decrease of the particles' size. This result is related to the formed droplets during the emulsification process [138]: the higher the stirring rate, the lower the droplets size. In fact, this droplets size is determined by the balance between the relative kinetics of the break-up and coalescence of the droplets, which are phenomena occurring simultaneously during emulsification and both influenced by the stirring rate [144].

Concerning the surfactant, studies [141, 146-148] have demonstrated that by augmenting the concentration of PVA, particles size decreases. PVA is a copolymer that usually acts as a stabilizer during the procedure of emulsification in different particles' preparation methods. This compound has influence both in the formed emulsification droplets and in the bulk solution: if in one hand the PVA can reduce interfacial tension, and induce mechanical and steric stabilization at the droplets' interface, where polymer chains interact, on the other hand, the non-adsorbed PVA chains contained in the bulk solution will influence the continuous phase viscosity, controlling the disruption kinetics of the droplets and promoting hydrodynamic stabilization. By lowering the interfacial tension at the droplets' interface, PVA allows a significant reduction in the energy required during emulsification. This tension reduction is mainly associated to PVA's amphiphilic character (the acetate groups constituted the hydrophobic part, while the hydroxyl ones correspond to the hydrophilic one) that allows PVA to be adsorbed and oriented at liquid-liquid interfaces, leading to the formation of a disperse system. Besides this stabilization, PVA can also cover completely the droplets, forming a firm anchoring at the interface and leading to the formation of a thick film. For this reason, it is possible for the polymer chains to have an optimal conformation into the external phase. Finally, the steric benefits arise from the short-range entropic repulsion between droplets, which is a result from the stabilization performed by PVA at the droplets surface [141].

Moreover, PVA plays an important role during the purification phase. Galindo-Rodriguez et al. [141] have studied the purification of particles by centrifugation and filtration, in order to assess the presence of residual PVA at the particles' surface. Their results show that, in both purification methods, there is a resistance of PVA to complete removal, suggesting that it is physically incorporated onto the particles surface. If on one side this may be advantageous for particles redispersion in water, as PVA hampers the particles' aggregation [141, 146], on the other hand it can alter the particles characteristics concerning specially their hydrophobicity and, therefore, their interaction with cells and cellular uptake [147]. Therefore, an equilibrium on PVA's concentration must be implemented.

Therefore, by increasing both PVA concentration and stirring rate, it was predictable to obtain smaller particles and vice versa. As a first attempt, these parameters were modified and the obtained results (Table VI) were in accordance with the expected. Yet, the obtained sizes in this first attempt were yet outside the predefined initial ranges. Therefore, further optimizations were performed (Table VII). However, as the presence of an extra compound in the mixture can alter the viscosity of the organic phase and, consequently, alter the stirring process, leading to differences in the final obtained sizes [149], this time particles were loaded with Coumarin-6. Coumarin-6 is a fluorescent marker, that, when entrapped inside the particles, confers a green color to them. By producing Coumarin-6 loaded particles, it is possible to track the particles destination when in contact with cells.

Table VI. PLGA particles size and preparation conditions. All PLGA particles were unloaded and were prepared by the Salting-out method, using the parameters specified in the Table. PVA concentrations used in the different phases of the procedure are here specified, where 1st step corresponds to the formation of the oil-in-water emulsion and 2nd step refers to the diffusion of the solvent into the aqueous phase. The column referred as purification presents the percentage of PVA used to purify the particles. Mean size and PDI results are demonstrated in the Obtained Mean Size and PDI columns, respectively. This characterization was performed right after the particles purification (i.e., particles were not freeze dried) by measurements performed by DLS. Results are presented as Average ± Standard Deviation (n=3, i.e., for each condition it was prepared one batch and for each batch 3 measurements were performed).

Experiment	1st step (% of PVA in wt/vol)	2nd step (% of PVA in wt/vol)	Stirring Rate ($\times 10^1$ rpm)	Purification (% of PVA in wt/vol)	Obtained Mean Size (nm)	PDI
A.I	5.00	0.500	2990	0.125	**355.0 ± 2.2**	0.109 ± 0.031
A.II	2.00	0.500	2045	0.125	**715.2 ± 99.1**	0.181 ± 0.024
A.III	0.50	0	1140	0.125	**2106.7 ± 307.2**	0.431 ± 0.344

Table VII. PLGA particles size after the optimization of the parameters in the preparation procedure. All the PLGA particles were loaded with 0.0300 % (wt/vol) of Coumarin-6 and were prepared by the Salting-out method, using the parameters specified in the Table. PVA concentrations used in the different phases of the procedure are here specified, where 1st step corresponds to the formation of the oil-in-water emulsion and 2nd step refers to the diffusion of the solvent into the aqueous phase. The column referred as purification presents the percentage of PVA used to purify the particles. Mean size and PDI results are demonstrated in the Obtained Mean Size and PDI columns, respectively. This characterization was performed right after the particles preparation (i.e., particles were not freeze dried) by measurements performed by DLS. Table is organized in an ascending order of obtained mean size. Results are presented as Average ± Standard Deviation (n=3, i.e., for each condition it was prepared one batch and for each batch 3 measurements were performed).

Experiment	1st step (% of PVA in wt/vol)	2nd step (% of PVA in wt/vol)	Stirring Rate ($\times 10^1$ rpm)	Purification (% of PVA in wt/vol)	Obtained Mean Size (nm)	PDI
B.I	8.00	0.500	2990	0.125	**265.4 ± 1.9**	0.091 ± 0.027
B.II	2.00	0.500	2990	0.125	**409.2 ± 0.3**	0.159 ± 0.014
B.III	2.00	0	2045	0	**1013.2 ± 40.4**	0.236 ± 0.022
B.IV	5.00	0.500	1445	0.125	**1041.0 ± 105.9**	0.504 ± 0.100
B.V	2.00	0	1445	0	**1944.0 ± 96.8**	0.273 ± 0.087

Experiment B.II (409.2 ± 0.3 nm) was considered optimized for the achievement of the Medium Particles (which were defined as particles with a size within the range from 400 to nm). Although Experiment B.III (1013.2 ± 40.4 nm) is above the mentioned range for the Large Particles (from 800 to 1000 nm), taking into account the result and its standard deviation, it was considered optimized for the mentioned group. Following the same reasoning, Experiment B.IV (1041.0 ± 105.9 nm) could also be considered as optimized for the Large Particles group. However, when comparing PDI values from both Experiments, condition B.III presented a lower value. PDI, as previously referred, is associated to the scattering of the size distribution on a particle suspension: it varies from 0 to 1, meaning that as closer to 0, the narrower is the particles' size distribution. Therefore, as PDI from Experiment B.IV (1041.0 ± 105.9 nm) was higher than the one obtained in Experiment B.III (1013.2 ± 40.4 nm), the latest's parameters were chosen as being optimized in detriment of the ones from Experiment B.IV (1041.0 ± 105.9 nm).

As it is observable, any of the experimented conditions produced particles for the range from 100 to 200 nm, which corresponded to the chosen interval for the Small Particles group. The closest to the defined range is the result obtained in Experiment B.I (265.4 ± 1.9 nm), which was performed with the maximum stirring rate conceivable. Therefore, as it was not possible to increase more the stirring rate, it was performed an attempt of augmenting the concentration of PVA in the 1st step from 8.00% (wt/vol) to 10.0% (wt/vol). However, the solution at 8.00% (wt/vol) of PVA was already near its saturation point due to the high concentration of $MgCl_2.H_2O$ hexahydratated. Consequently, the solutes had precipitated when the concentration of PVA was raised to 10.0% (wt/vol). Also, a high concentration of PVA is undesirable, as this compound is potentially carcinogenic and, as previously mentioned, it can alter the characteristics associated to particles' cellular uptake [147, 150].

Taking into account the aforementioned considerations, it was decided that other method should be studied for the development of the Small Particles (with a range between 100 and 200 nm). Therefore, Nanoprecipitation method was studied as the method for obtaining the smaller particles, necessary for the internalization studies. In order to assess the most suitable parameters for the preparation of particles by nanoprecipitation, both the organic solvent and the purification method were varied, being the obtained results present in Figure 6.

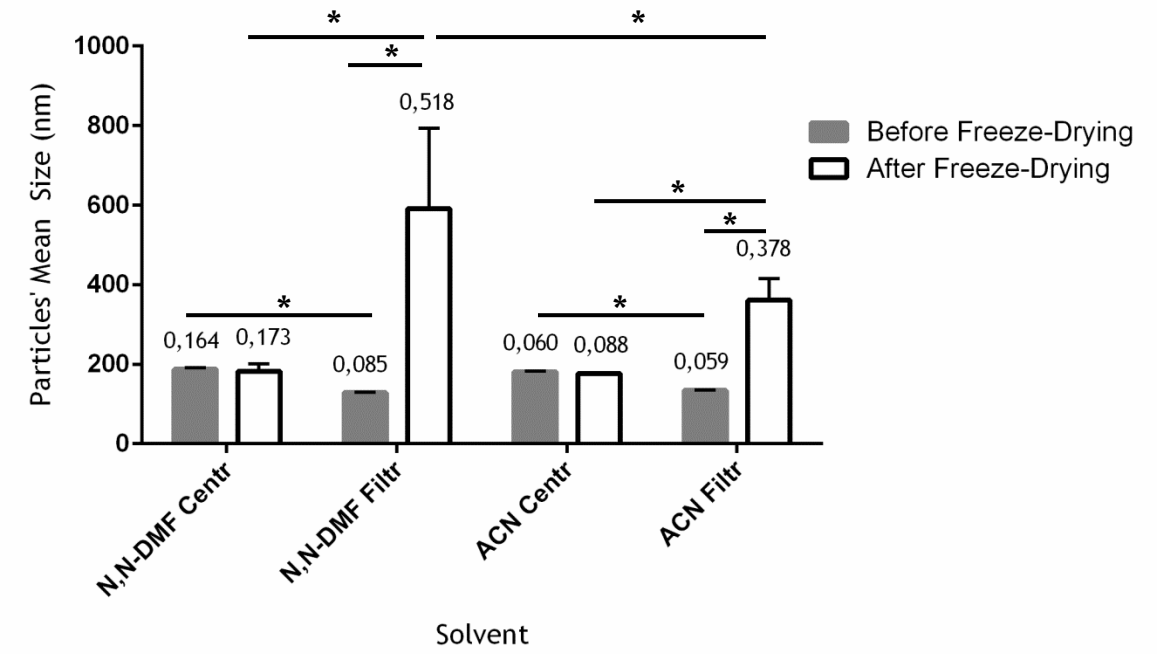

Figure 6. Size of the particles prepared with the nanoprecipitation method. The preparation procedure was performed using N,N-Dimethylformamide (N,N-DMF) or Acetonitrile (ACN). The purification of the particles was performed either by centrifugation (Centr), with resuspension in a solution of 0.125% (wt/vol) of PVA, or Filtration (Filtr). Both size and PDI values were obtained by measurements performed in DLS. Results are presented as Average ± Standard Deviation (n=3, i.e., for each condition it was prepared one batch and for each batch 3 measurements were performed). At the top of each bar is represented the mean PDI values for each group.. * Particles' size was significantly different between the signaled conditions, considering $p \leq 0.05$.

Results show significant differences between particles prepared with different solvents and different purification methods, both before and after Freeze-Drying.

Once the organic solvent is modified, the polymer-solvent and water-solvent interactions become different, inducing changes in the particles' mean size [141]. Concerning the water-solvent interactions, their influence on the particles' mean size may be explained by the solubility of the solvents: the higher the solubility, the more efficient is the solvent diffusion into the aqueous phase. Furthermore, as the polymer is usually transported by the solvent, with higher solvent solubility the polymeric chains will be partitioned more efficiently in the external phase, forming aggregates and, consequently, particles [136, 141]. As DMF is a more water miscible solvent than ACN, it was expected that the mean size of the particles was lower in the samples prepared with DMF [136]. However, differences were only found between the samples prepared by DMF and purified by filtration, which presented a size of 591.3 ± 165.0 nm, and the particles prepared with ACN and also purified by filtration, which presented a size of 361.0 ± 44.5 nm. Therefore, these results were not in agreement with the expected, meaning that other factors, such as the Freeze-Drying procedure or the purification method, may have introduced variables on the procedure, leading to these non-expected differences.

Freeze-drying is one of the most suitable methods to stabilize and facilitate the handling of colloidal systems, which otherwise would be stored as suspensions [151]. It allows the removal of the particles solvent, resulting on dried particles. Although it is appropriate for preserving

the original properties of particles, this procedure may bring some problems to the system, giving rise to the loss of integrity of the particles' characteristics [91, 151]. For instance, ice crystallization may exert mechanical stress on particles leading to a destabilization. On the other hand, when the particles concentration is too high, freeze-drying may favor aggregation or irreversible coalescence of particles [91]. Therefore, it is important to find ways that may circumvent these problems, being one of the most used solutions the addition of cryoprotectants. Cryoprotectants can both improve the resistance of particles towards freezing and drying stresses, as well as the stability for long term storage. Sugars are the most popular cryoprotectants and, although their effect is mostly benefic, the ratio between cryoprotectant/particles is an important parameter, as above an optimal value, particles stability can be compromised [91]. Diana Leite [93] has optimized the procedure for a sugar : particles mass ratio of 2:1. Although it the referred study it was optimized the usage of glucose as a cryoprotectant for PLGA particles, sucrose is a disaccharide, therefore leading to the formation of a more complex glassy matrix around particles during the Freeze-Drying and, consequently, to a more efficient protection. For this reason, sucrose was used as a cryoprotectant for the particles at a ratio of 2:1, for the samples purified by centrifugation. Regarding the nanoparticles purified by filtration, their weight was not controlled and, therefore, it was not possible to formulate the ratio. For this reason, particles purified by filtration did not have any cryoprotectant that could stabilize them. Furthermore, during the purification phase, the particles purified by filtration, contrary to what occurred with the particles purified by centrifugation, were not resuspended in a solution of 0.125% (wt/vol) of PVA. As previously referred, PVA is resistant to its complete removal [141], forming a layer at the particles' surface. This layer becomes advantageous at the time of resuspending the particles in water, after Freeze-Drying: it leads to the formation of fewer aggregates and, therefore, to a more effective stabilization of the particles' size. Therefore, due to the absence of a cryoprotectant and PVA during Freeze-Drying, there was an aggregation phenomenon on the particles purified by filtration, leading to the significantly different results: for particles prepared with DCM and purified by filtration, the results showed a size of 128.8 ± 1.2 nm before Freeze-Drying and 591.3 ± 165.0 nm after it; for particles prepared with ACN and also purified by filtration, the measured sizes corresponded to 134.2 ± 1.6 nm before Freeze-Drying and to 361.0 ± 44.5 nm after it.

When a comparison is performed between the two methods of purification, significant differences can also be found. Before Freeze-Drying, particles prepared with DMF and purified by centrifugation presented a size of 187.4 ± 4.7 nm, while the ones prepared with the same solvent but purified by filtration showed a size of 128.8 ± 1.2 nm; the particles prepared with ACN and purified by centrifugation revealed a size of 180.9 ± 3.5 nm, while the ones prepared with the same solvent but purified by filtration had a size of 134.2 ± 1.6 nm. This may be associated with the presence of particles aggregates: although PVA is present in solution, giving

stabilization to the particles, the centrifugation procedure may lead to an incomplete removal of aggregates and coalesced particles. Contrarily to what happens in the filtration procedure, centrifugation does not warranty the elimination of all particles with a diameter above a well-defined size, as the aggregates will sediment with the particles [91]. This will lead to the presence of larger particles in suspension when compared to the filtration purification procedure. However, when comparisons are performed after Freeze-Drying, an opposite situation occurs: particles prepared with DMF and purified by centrifugation presented a size of 182.5 ± 15.3 nm, while the ones prepared with the same solvent but purified by filtration had a size of 591.3 ± 165.0 nm; regarding the particles prepared with ACN purified by centrifugation, these showed a size of 176.8 ± 1.0 nm, while the ones purified by filtration revealed a size of 361.0 ± 44.5 nm. These larger sizes associated with particles purified by filtration is related to the Freeze-Drying procedure that induced changes in the particles, as above described.

Therefore, taking into consideration all the results showed, the solvent ACN and purification by centrifugation, were the selected parameters for the preparation of particles of smaller sizes. Although there were not significant differences between particles prepared with ACN and DMF and purified by centrifugation, the reason behind the selection of ACN in detriment of DMF relies on the PDI. PDI presents higher values on the samples prepared by DMF, when compared to the ones prepared by ACN. As the lower the PDI value, the narrower the distribution of sizes, ACN samples were considered more suitable for the pretended application, presenting a mean size of 180.9 ± 3.5 nm and 176.8 ± 1.0 nm before and after Freeze-Drying, respectively, which is within the predefined initial range for the Small particles (range from 100 to 200 nm).

Once all the pretended sizes were obtained after optimization, it was possible to test the particles cytotoxicity and their internalization in mice BMC. Table VIII shows the obtained sizes for each group of particles used in the following experiments.

Table VIII. Sizes and respective PDI results for the particles used in the cytotoxic assessment and internalization studies after 3 and 7 days of cell culture differentiation. These particles were prepared accordingly to the previous optimized parameters. Results are presented as Average ± Standard Deviation (n=3, i.e., for each condition it was prepared one batch and for each batch 3 measurements were performed).

	Small Particles		Medium Particles		Large Particles	
	Size (nm)	PDI	Size (nm)	PDI	Size (nm)	PDI
3 Days	188.0 ± 4.8	0.112 ± 0.059	430.0 ± 10.1	0.160 ± 0.012	802.6 ± 48.7	0.285 ± 0.012
7 Days	195.2 ± 0.0	0.078 ± 0.015	417.4± 11.0	0.162 ± 0.069	954.6 ± 31.7	0.220 ± 0.032

4.2. Particles Cytotoxicity

Cell viability was evaluated by Live/Dead assay, where cells marked with the Calcein AM (a green fluorescent dye for viable cells) were considered as being alive and the ones marked with Propidium Iodide (a red fluorescent dye for dead cells) were considered as being dead. In order to have representative results for each condition, three different areas in each well were considered for the counting. Regarding cell metabolic activity, a Resazurin assay was performed. Here, considering the control constituted only by BMC as having 100% of metabolic activity, the percentages of metabolic activity for the other conditions were calculated. Results for cells after 3 and 7 days of culture are represented in Figure 7 and 8, in which A corresponds to the Live/Dead results and B to the Resazurin ones.

No differences were found in cell viability. In what concerns cell metabolic activity, no differences were also found between the samples and the control containing only BMC. However, to consider a material as being non-cytotoxic, the restrictions imposed by ISO 10993-5 [152] consider that the metabolic activity of the cells must be maintained above 70%. This percentage was not reached by all the conditions, as the average metabolic activity was below 70% for Coumarin-6 cultured alone with cells, in both days, and for the Small Particles cultured with cells after 3 days of culture. Coumarin-6 has been used at higher concentrations without showing toxicological results [153]. However, this compound hardly dissolved on the cell culture medium at the time of incubation, and, although its concentration was low (0.0006% wt/vol), there was a presence of small Coumarin-6 aggregates. As reported by Yu Pan et al. [154], nanoparticles are of similar size to typical cellular components and proteins, having the capability of bypassing natural mechanical barriers and, consequently, lead to adverse tissue reactions. Moreover, when particles are too small, they are endocytosed, instead of phagocyted [155, 156], which may result on the binding of particles to intracellular targets, causing disturbance on cellular signaling, motility and metabolism [154]. For this reason, and considering the aggregates of Coumarin-6 as also being small particles, both Coumarin-6 and Small Particles may have been taken by cells through endocytosis, inducing changes in metabolic activity and, therefore, revealing lower percentages as presented. However, if standard deviations are considered, all showed results present values above 70%, meaning that further studies must be performed in this topic in order to confirm the presented results.

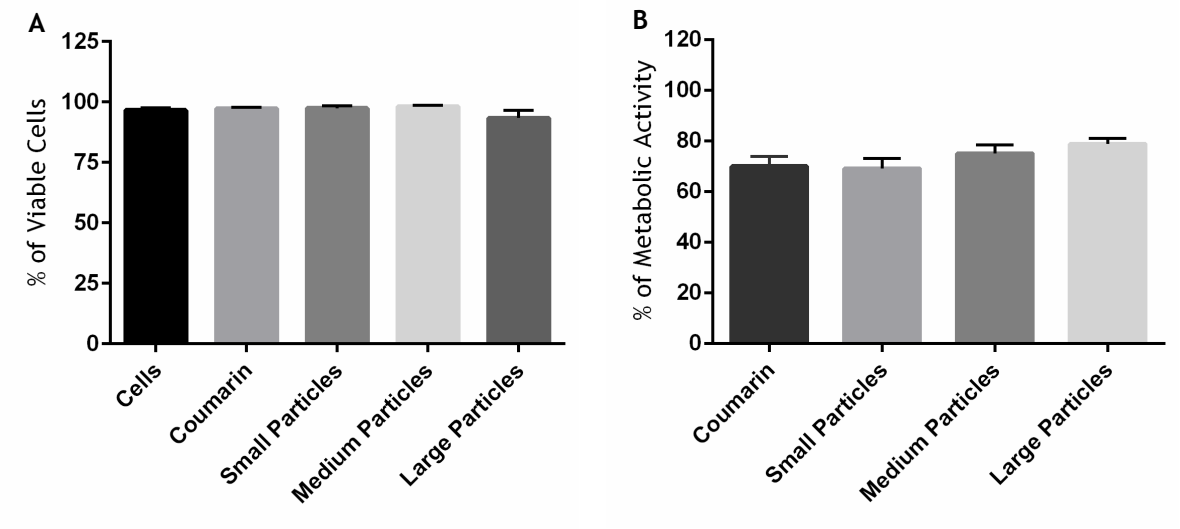

Figure 7. Particles Cytotoxicity results for BMC after 3 days of differentiation and upon 3 hours of incubation with Coumarin-6 loaded particles. These results were assessed by (A) Live/Dead assay and (B) Resazurin assay. In the Live Dead assay (A), results were assessed by analyzing three different areas in each condition. Viable cells were stained with Calcein AM, presenting a green colour, and dead cells were colored as red by Propidium Iodide. Regarding the Resazurin Assay (B), the percentage of metabolic activity for each condition was calculated considering cells alone as having 100% of metabolic activity. Results are presented as Average ± Standard Deviation (n=1 for A and n=2, i.e., using the same cells, 2 replicas could be evaluated, for B). Statistical analysis was performed for the results from the Resazurin assay, but no differences were found between the conditions and the control containing only cells. Due to n being only equal to 1, no statistical analysis was performed for the Live/Dead assay.

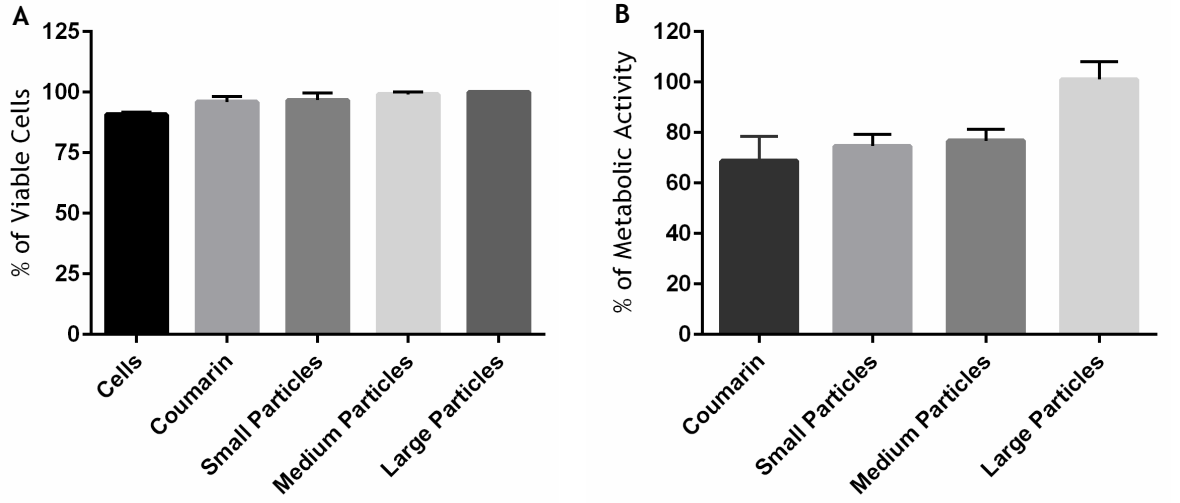

Figure 8. Particles Cytotoxicity results for BMC after 7 days of differentiation and upon 3 hours of incubation with Coumarin-6 loaded particles. These results were assessed by (A) Live/Dead assay and (B) Resazurin assay. In the Live Dead assay (A), results were assessed by analyzing three different areas in each condition. Viable cells were stained with Calcein AM, presenting a green color, and dead cells were colored as red by Propidium Iodide. Regarding the Resazurin Assay (B), the percentage of metabolic activity for each condition was calculated considering cells alone as having 100% of metabolic activity. Results are presented as Average ± Standard Deviation (n=1 for A and n=2, i.e., using the same cells, 2 replicas could be evaluated, for B). Statistical analysis was performed for the results from the Resazurin assay, but no differences were found between the conditions and the control containing only cells. Due to n being only equal to 1, no statistical analysis was performed for the Live/Dead assay

4.3. Evaluation of the Internalization

BIBP3226 has been studied on our team has a potent antagonist for Y1 receptor. Recently a member of our team, Francisco Conceição, has performed works *in vitro* using BIBP3226 administrated alone in monocultures and co-cultures of osteoblasts with osteoclasts. However, by the time of this project planning, only osteoclasts had revealed conclusive results, showing a lower capacity of resorption in the presence of BIBP3226. As in a future work it is aimed to load the PLGA particles with BIBP3226 and assess the efficiency of the drug delivery system, it was decided that the internalization studies should be performed in osteoclasts, as the readout for BIBP3226 effect in these cells was already knew. Therefore, the protocol used here to prepare the cell culture was the one used by Francisco Conceição, who has confirmed the presence of osteoclasts by performing Tartrate-resistant acid phosphatase (TRAP) staining, TRAP release quantification and Real Time Polymerase Chain Reaction (RT-PCR) for genes that typify the osteoclast lineage (cathepsin K, osteoclast-associated receptor and calcitonin receptor). However, as in this project it was not used any marker to verify the presence of osteoclasts, cells with a number of nuclei between 2 to 13 will be referred as multinucleated cells. For the same reason, cells with only one nucleus will be referred as mononucleated cells.

In a first attempt, it was projected that the internalization studies should be assessed by Fluorescence Activated Cell Sorting (FACS). However, due to the low quantity of cells, this procedure could not be performed. Therefore, analysis by Image Flow Cytometry was executed (data not shown); however Coumarin-6 presents a high fluorescence that did not allow the distinction between particles and background. Therefore, these two techniques were discarded and internalization was assessed by Image Analysis, using images taken in an Inverted Fluorescence Microscope. In order to both evaluate cell morphology and particles internalization, F-actin filaments were stained in red and the cellular nuclei were marked in blue. Results were assessed after 3 hours of incubation with the previously prepared Coumarin-6 loaded particles, with the sizes referred in Table VIII.

Regarding the quantity of multinucleated cells, it is observed that after 3 days of culture (Figure 9) the amount of multinucleated cells was lower than after 7 days of culture (Figure 10). If it is assumed that, although markers were not used, the majority of the multinucleated cells correspond to osteoclasts, then the results are in agreement with literature, as usually the majority of the osteoclastogenesis occurs after 7-8 days of culture [157].

In order to evaluate the particles' internalization, firstly the percentage of internalization was calculated. In order to calculate this parameter, 6 images (like the representative ones in Figure 9 and Figure 10, for the time points of 3 and 7 days, respectively) from different areas were analyzed in each condition. By evaluating the cells that had internalized particles, a percentage could be calculated (Table IX and X that allowed to construct the graphs in Figure 11- A and Figure 11-B, for the time points of 3 and 7 days, respectively). The results show that less than 50.0% of cells had internalized particles. In what concerns the capacity of

internalization, it was observed that mononucleated cells have increased their capacity of internalization from the time point of 3 days to the time point of 7 days. In what concerns the multinucleated cells, the capacity of uptaking the large particles has decreased with the increase of days of culture. The contrary situation happened with the medium particles, as the multinucleated cells increased the capacity of internalizing these sized particles from the time point of 3 to the one of 7 days.

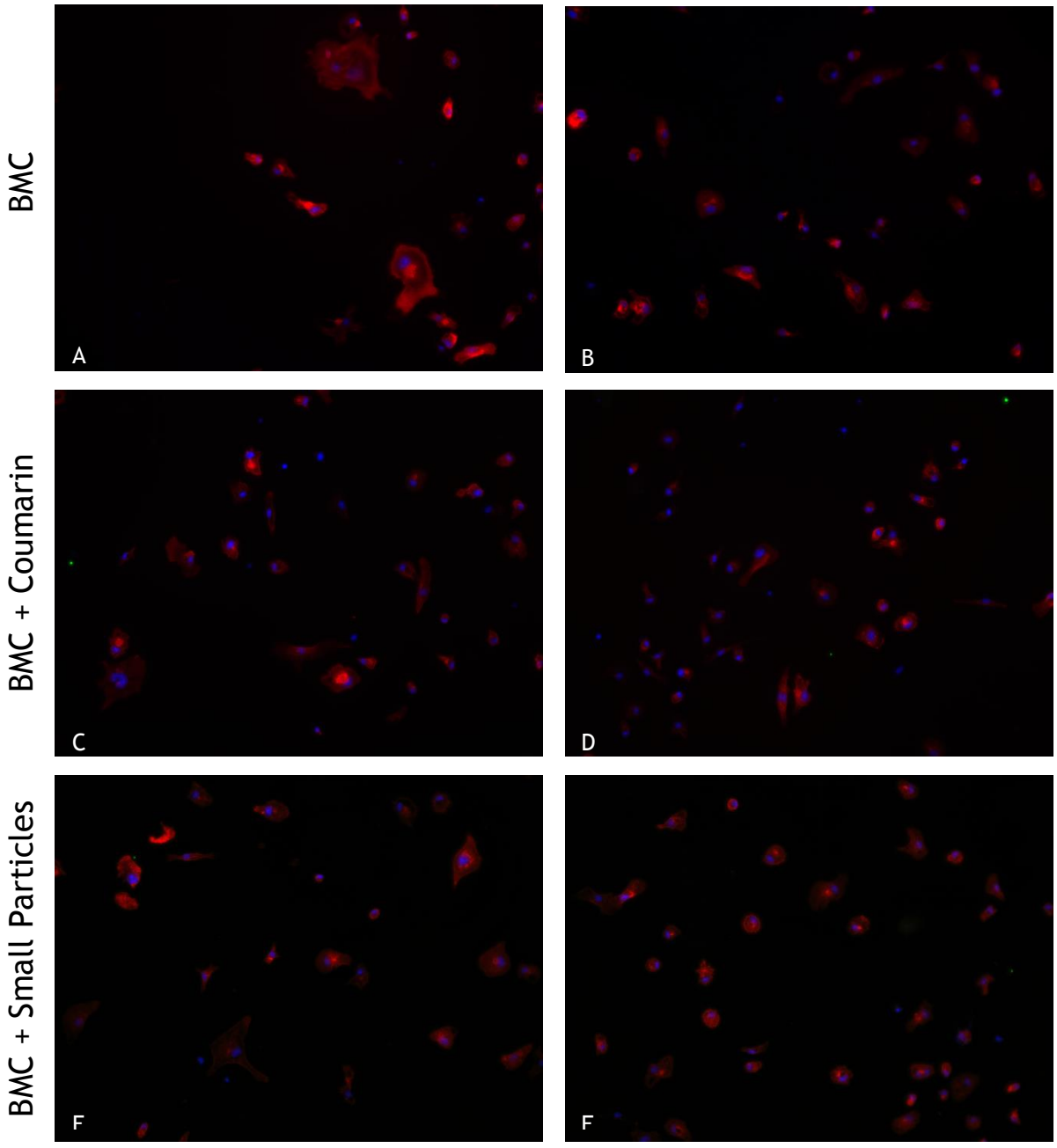

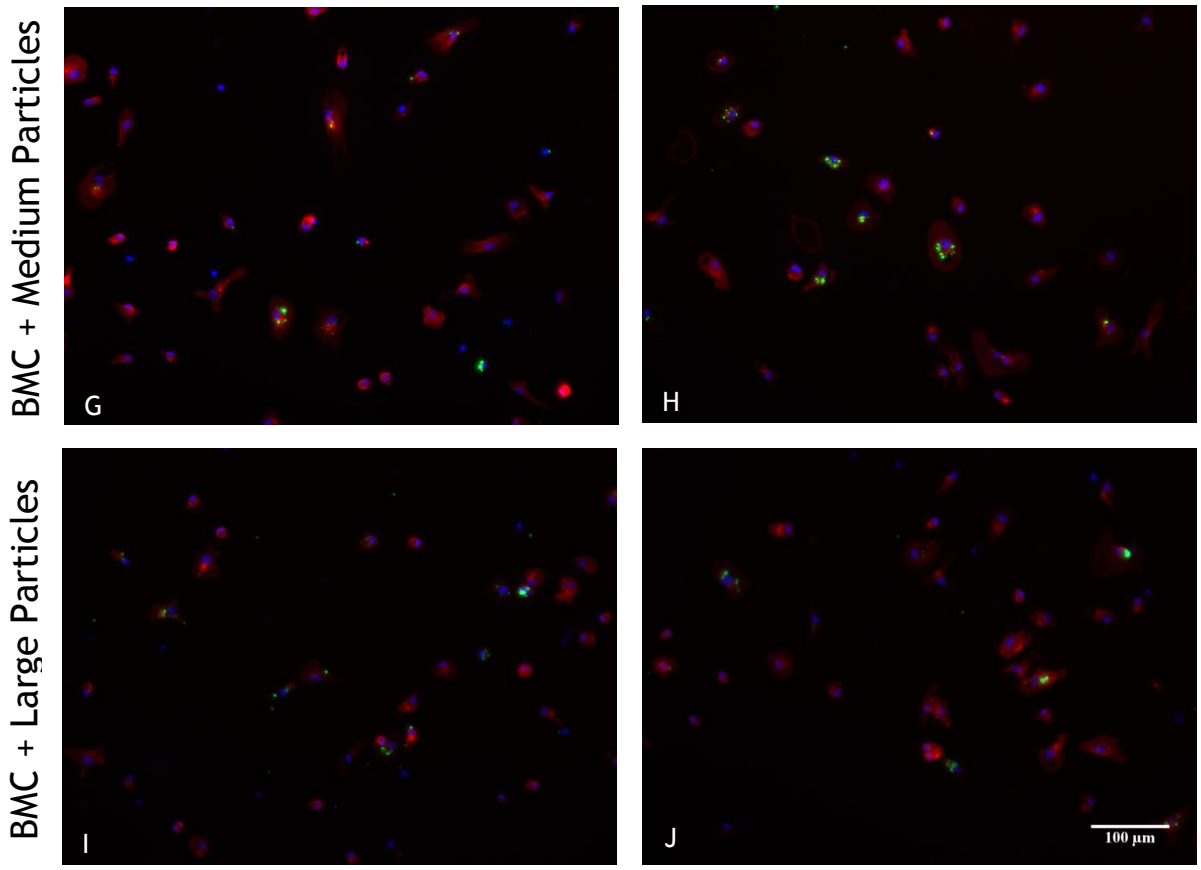

Figure 9. Representative fluorescent micrographs showing Bone Marrow derived Osteoclast Lineage Cells (BMC) after 3 days of culture and upon 3 hours of incubation with Coumarin-6 loaded particles. Images show fixed and permeabilized BMC either cultured alone (A and B), with 0.000600% (wt/vol) Coumarin-6 (C and D) and with 0.0400% (wt/vol) of Small (E and F), Medium (G and H) and Large (I and J) particles. Particles had an average size of 188 nm (Small Particles), 430 nm (Medium Particles) and 802 nm (Large Particles). F-actin filaments are stained in red, cells' nuclei are stained in blue and both Coumarin-6 and particles are represented in color green. Scale bar: 100 µm.

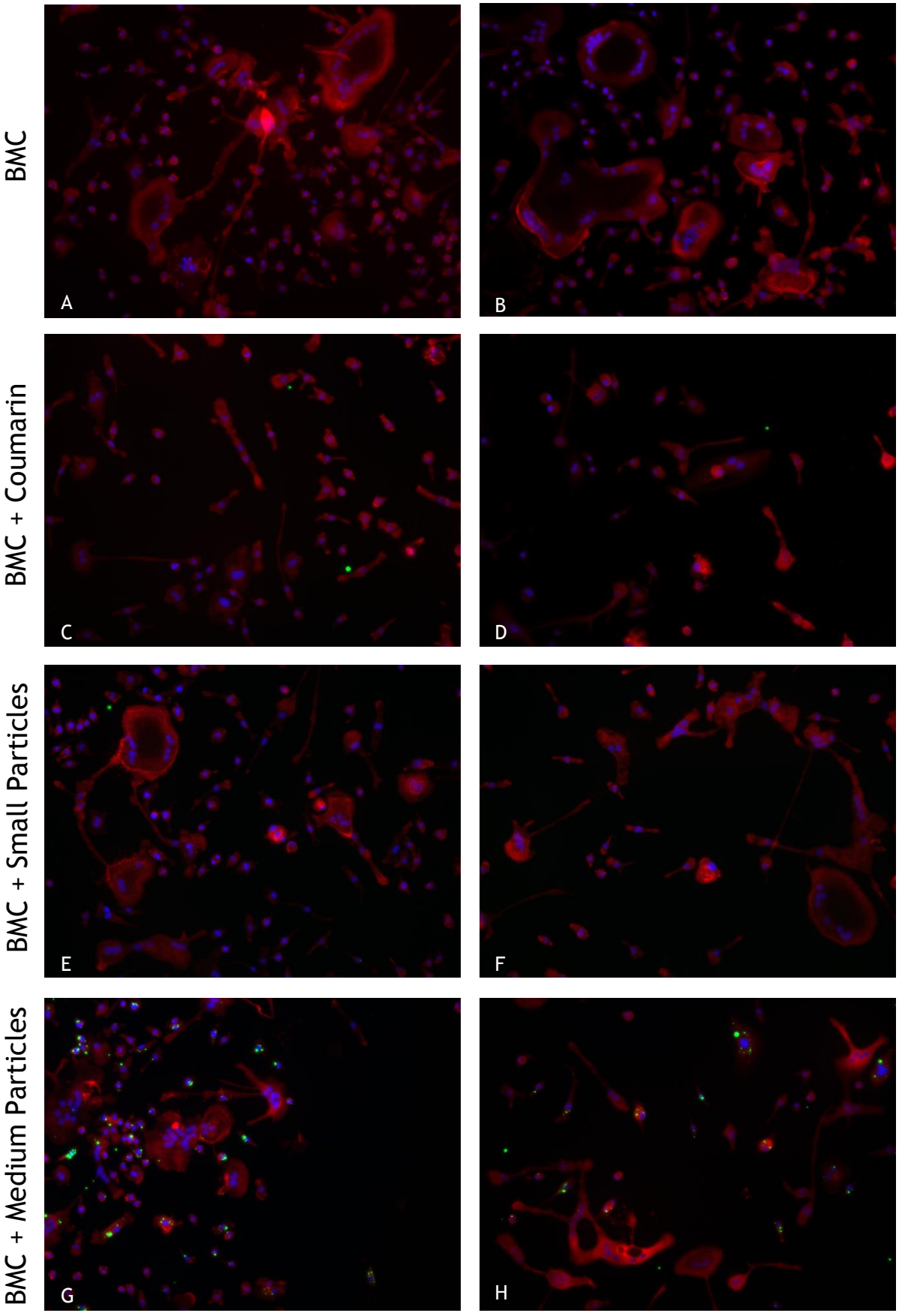
BMC
BMC + Coumarin
BMC + Small Particles
BMC + Medium Particles
A
B
C
D
E
F
G
H

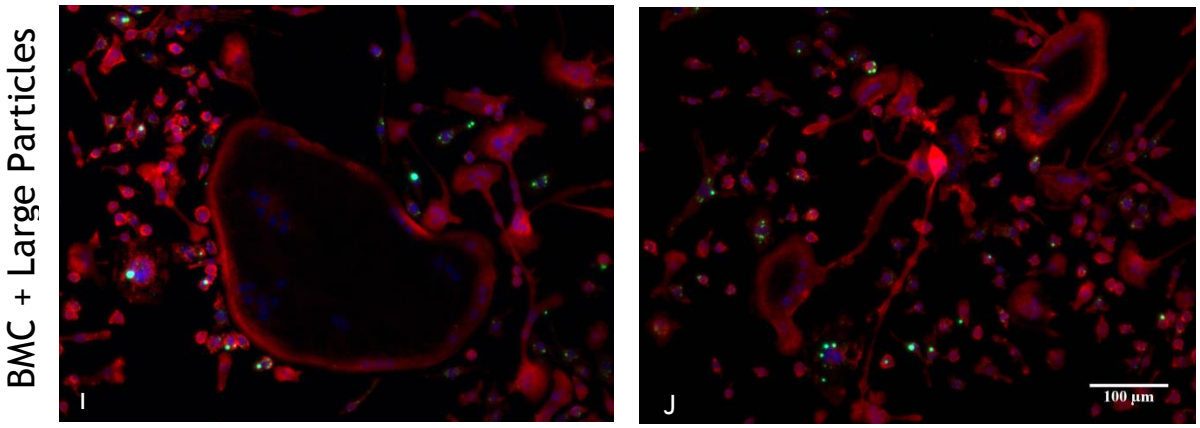

Figure 10. Representative fluorescent micrographs showing Bone Marrow derived Osteoclast Lineage Cells (BMC) after 7 days of culture and upon 3 hours of incubation with Coumarin-6 loaded particles. Images show fixed and permeabilized BMC either cultured alone (A and B), with 0.000600% (wt/vol) Coumarin-6 (C and D) and with 0.0400% (wt/vol) of Small (E and F), Medium (G and H) and Large (I and J) particles. Particles had an average size of 195 nm (Small Particles), 417 nm (Medium Particles) and 955 nm (Large Particles). F-actin filaments are stained in red, cells' nuclei are stained in blue and both Coumarin-6 and particles are represented in color green. Scale bar: 100 µm.

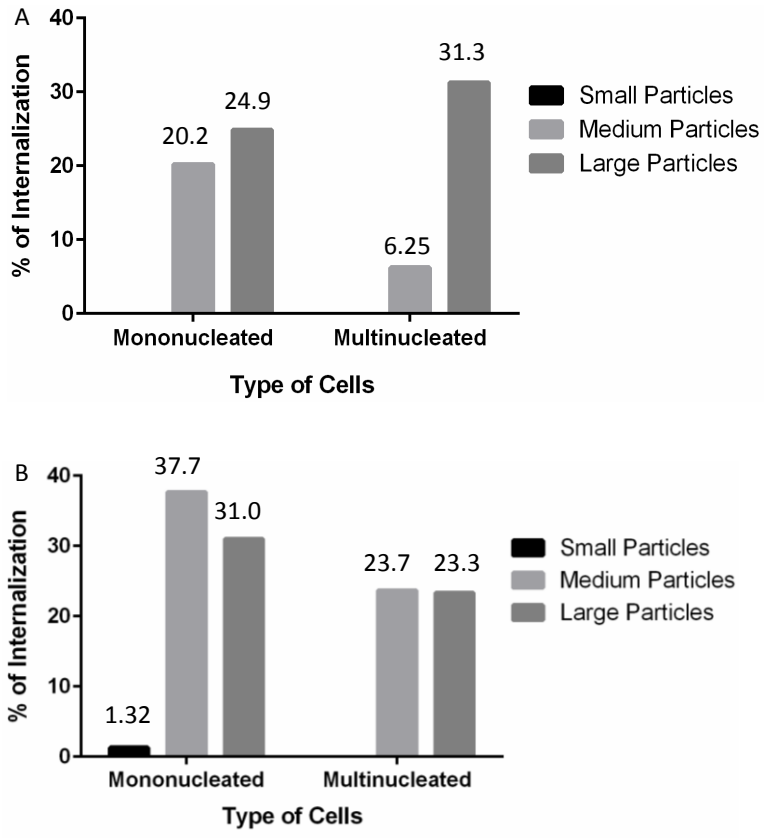

Figure 11. Percentage of Internalization of Coumarin-6 loaded particles, upon 3 hours of incubation, in mono and multinucleated cells cultured for 3 days (A) and 7 days (B). Illustrative results from Table IX and Table X, respectively. The correspondent values of the bars are represented at the top of them.

Table IX. Percentage of Internalization of Coumarin-6 loaded particles, upon 3 hours of incubation, in mono and multinucleated cells cultured for 3 days. Results were obtained by assessing 6 different spots in the well per condition (as described earlier in Figure 9). It was considered that cells had internalized particles in all instances where particles were co-localized with the F-actin filaments. Cells and cells with Coumarin-6 served as controls to evaluate the effect of Coumarin-6 and the particles in cells.

		Total of Cells Containing Particles	Total of Cells Without Particles	Percentage of Internalization (%)
Small Particles	Mononucleated	0	182	**0**
	Multinucleated	0	9	**0**
Medium Particles	Mononucleated	36	142	**20.2**
	Multinucleated	1	15	**6.25**
Large Particles	Mononucleated	44	133	**24.9**
	Multinucleated	5	11	**31.3**

Table X. Percentage of Internalization of Coumarin-6 loaded particles, upon 3 hours of incubation, in mono and multinucleated cells cultured for 7 days. Results were obtained by assessing 6 different spots in the well per condition (as described earlier in Figure 11). It was considered that cells had internalized particles in all instances where particles were co-localized with the F-actin filaments. Cells and cells with Coumarin-6 served as controls to evaluate the effect of Coumarin-6 and the particles in cells.

		Total Number of Cells Containing Particles	Total Number of Cells Without Particles	Percentage of Internalization (%)
Small Particles	Mononucleated	3	225	**1.32**
	Multinucleated	0	51	**0**
Medium Particles	Mononucleated	81	134	**37.7**
	Multinucleated	9	29	**23.7**
Large Particles	Mononucleated	115	256	**31.0**
	Multinucleated	14	46	**23.3**

As Small particles were difficult to be visualized, 10 images (like the representative ones present in Figure 12 and Figure 13, which represent the cell culture after 3 and 7 days respectively) per condition, and from different areas of each well, were observed and analyzed at higher magnifications. By assessing these images and by only analyzing the cells that had internalized, the number of particles per cell was calculated (Table XI and XII, which allowed to construct Figure 14-A and Figure 14-B for the time points of 3 and 7 days respectively). The results show that for mononucleated cells the number of particles per cell was maintained, with exception for the Large particles. In what concerns the multinucleated cells, there was a

decrease in the number of particles per cell from one time point to another, excluding the Small particles, for which there was an increase in the average number per cell.

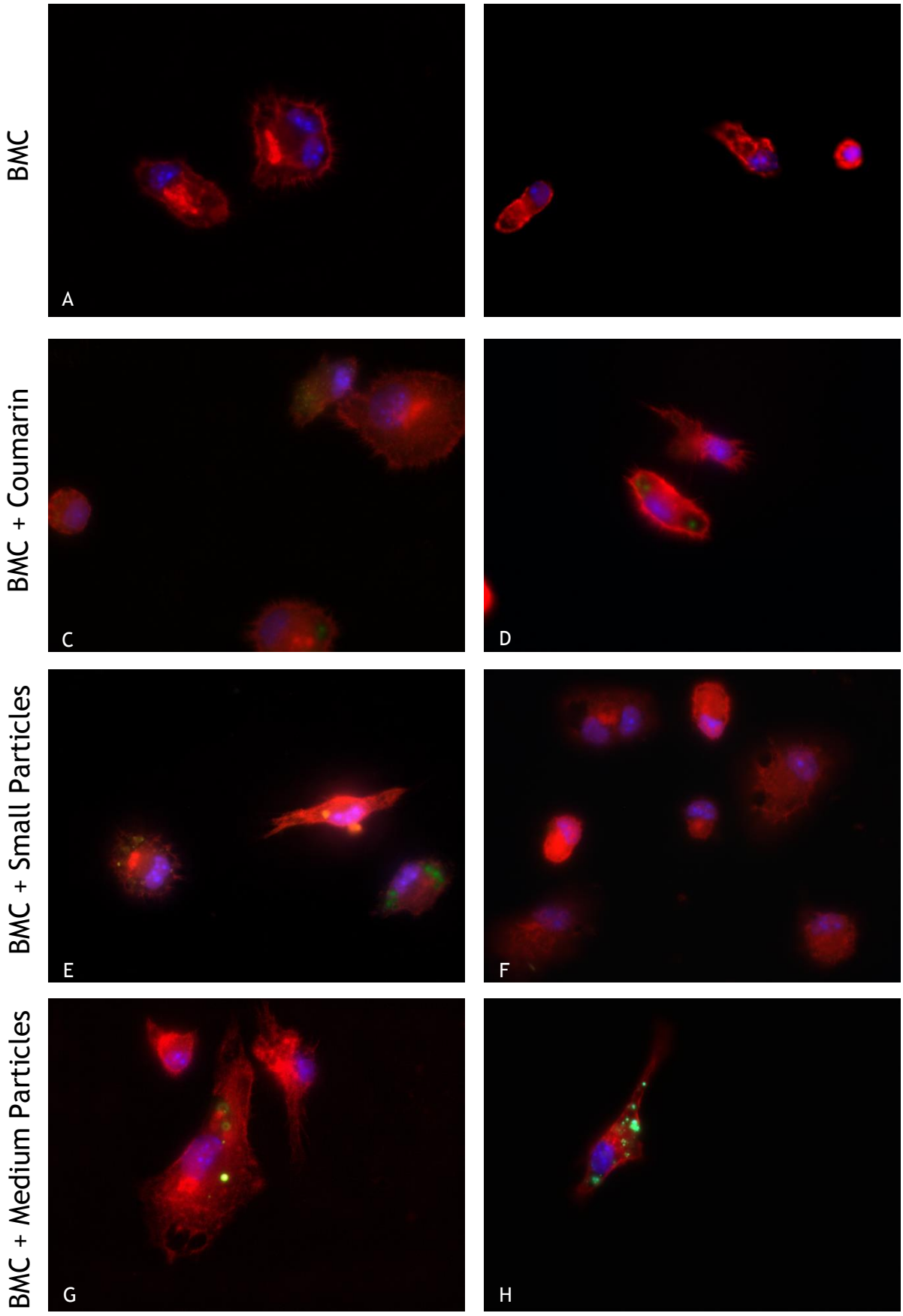

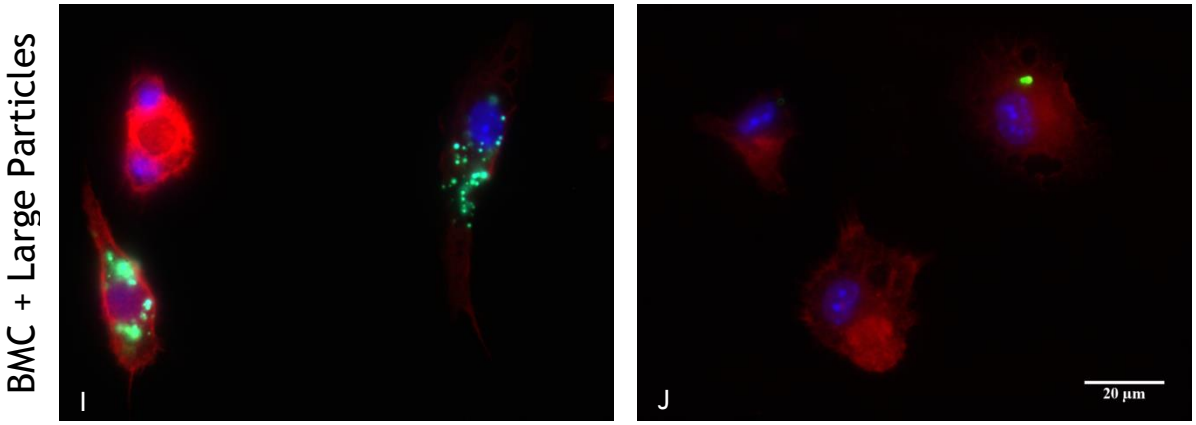

Figure 12. Representative fluorescent micrographs showing Bone Marrow derived Osteoclast Lineage Cells (BMC) after 3 days of culture and upon 3 hours of incubation with Coumarin-6 loaded particles. Images show fixed and permeabilized BMC cultured alone (A and B), with 0.000600% (wt/vol) Coumarin-6 (C and D) and with 0.0400% (wt/vol) of Small (E and F), Medium (G and H) and Large (I and J) particles. Particles had an average size of 188 nm (Small Particles), 430 nm (Medium Particles) and 802 nm (Large Particles). F-actin filaments are stained as red, cells' nuclei are stained in blue and both Coumarin-6 and particles are represented in the color green. Scale bar: 20 μm.

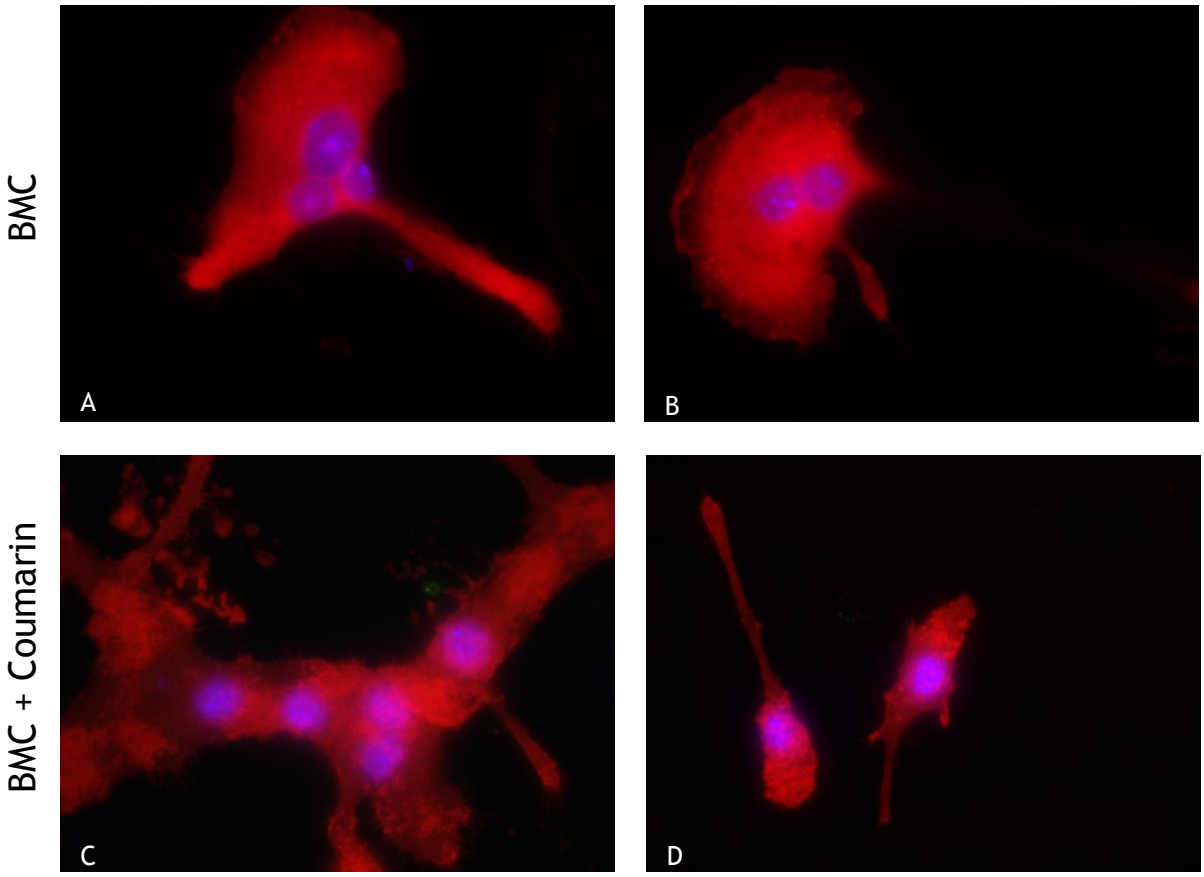

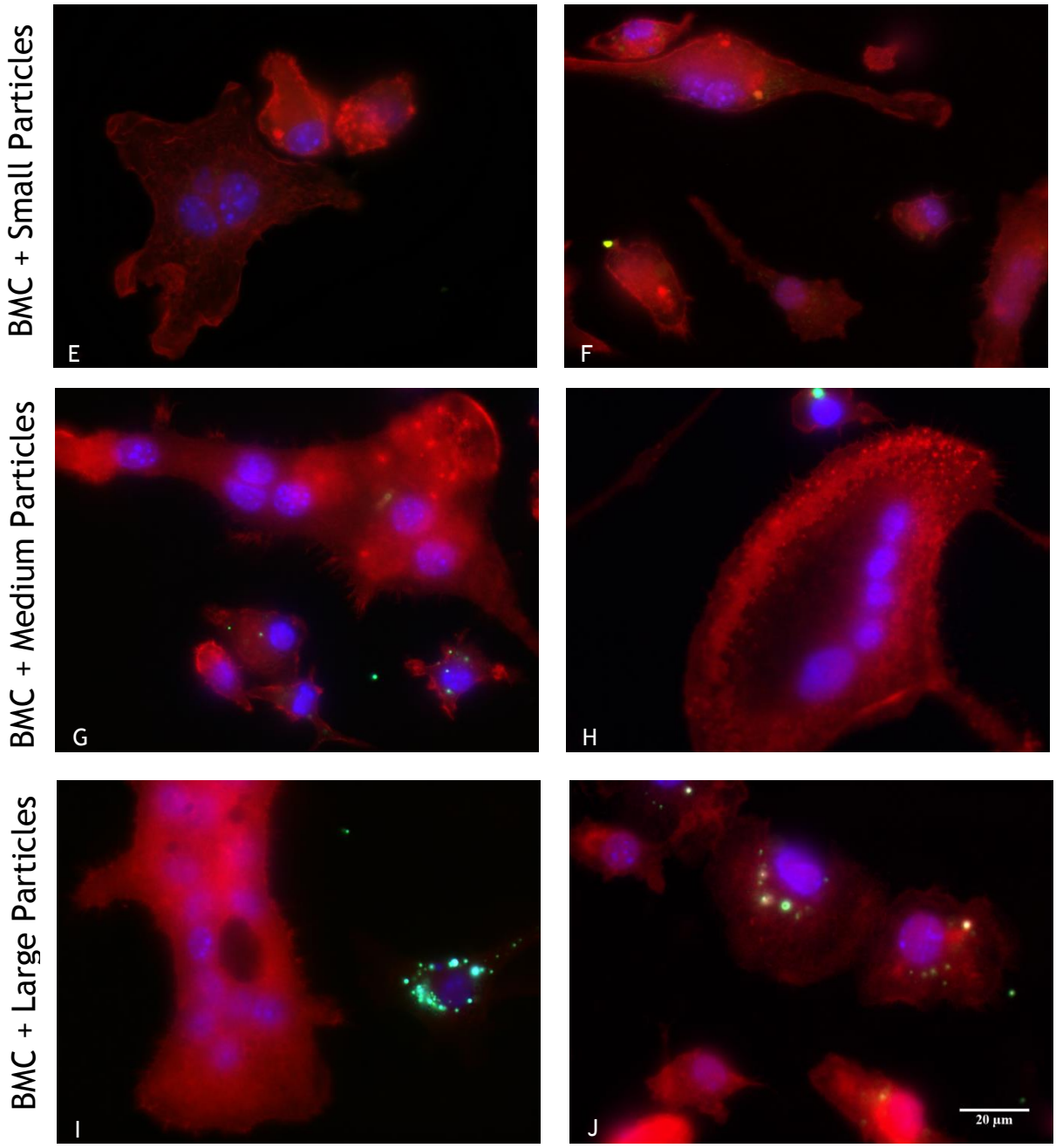

Figure 13. Representative fluorescent micrographs showing Bone Marrow derived Osteoclast Lineage Cells (BMC) after 7 days of culture and upon 3 hours of incubation with Coumarin-6 loaded particles. Images show fixed and permeabilized BMC either cultured alone (A and B), with 0.000600% (wt/vol) Coumarin-6 (C and D) and with 0.0400% (wt/vol) of Small (E and F), Medium (G and H) and Large (I and J) particles. Particles had an average size of 195 nm (Small Particles), 417 nm (Medium Particles) and 955 nm (Large Particles). F-actin filaments are stained in red, cells' nuclei are stained in blue and both Coumarin-6 and particles are represented in the color green. Scale bar: 20 μm.

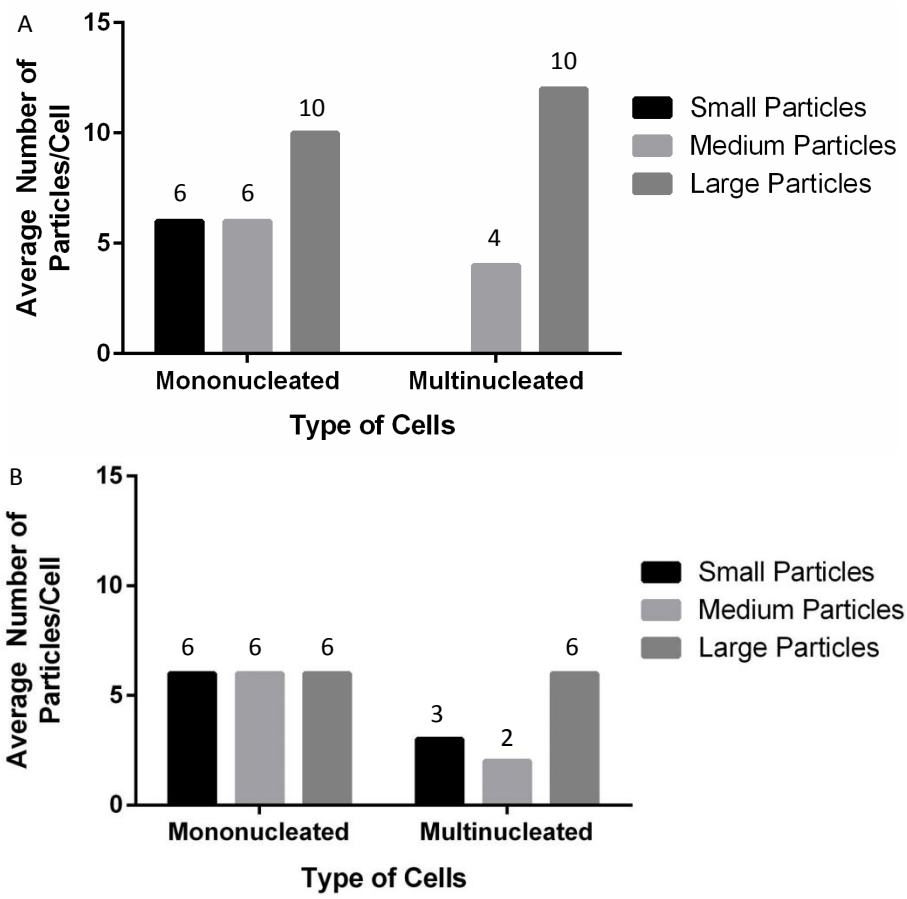

Figure 14. Average number of internalized Coumarin-6 loaded particles, upon 3 hours of incubation, per mono and multinucleated cell after 3 days (A) and 7 days (B) of incubation. Illustrative results from Table XI and XII, respectively. The correspondent values of the bars are represented at the top of them.

Table XI. Average number of internalized Coumarin-6 loaded particles, upon 3 hours of incubation, per mono and multinucleated cell after 3 days of culture. Results were obtained by assessing 10 different spots in the well per condition (as described earlier in Figure 13). It was considered that cells had internalized particles in all instances were particles were co-localized with the F-actin filaments. Cells and cells with Coumarin-6 served as controls to evaluate the effect of Coumarin-6 and the particles in cells.

		Total of Cells Containing Particles	Total of Counted Particles	Average of Particles/Cell
Small Particles	Mononucleated	7	40	**6**
	Multinucleated	0	0	**0**
Medium Particles	Mononucleated	11	63	**6**
	Multinucleated	1	4	**4**
Large Particles	Mononucleated	10	100	**10**
	Multinucleated	1	12	**12**

Table XII. Average number of internalized Coumarin-6 loaded particles, upon 3 hours of incubation, per mono and multinucleated cell after 7 days of culture. Results were obtained by assessing 10 different spots in the well per condition (as described earlier in Figure 13). It was considered that cells had internalized particles in all instances were particles were co-localized with the F-actin filaments. Cells and cells with Coumarin-6 served as controls to evaluate the effect of Coumarin-6 and the particles in cells.

		Total of Cells Containing Particles	Total of Counted Particles	Average of Particles/Cell
Small Particles	**Mononucleated**	3	17	**6**
	Multinucleated	4	13	**3**
Medium Particles	**Mononucleated**	21	118	**6**
	Multinucleated	4	8	**2**
Large Particles	**Mononucleated**	28	154	**6**
	Multinucleated	11	67	**6**

Osteoclasts are considered as being part of the mononuclear phagocyte system (MPS) [158]. These cells are formed by fusion of circulating mononuclear precursor cells of hematopoietic origin, having precursors in common with monocytes and macrophages, which also belong to the MPS [158]. As reviewed on literature, although for non-phagocytic cells it is clear that the larger the particles, the lower the internalization, for phagocytic cells there is no clear evidence that internalization is unequivocally related to the particles size [106]. Moreover, it is hypothesized that an optimum particle size to avoid internalization relies between 200 and 500 nm [108], as particles below 200 nm are internalized by receptor mediated endocytosis and the ones higher than 500 nm are phagocyted [155, 156]. However, the results do not show these conclusions, as for the Small particles the internalization was lower. This may be associated to the increased difficulty in observing the Small particles. In order to overcome this problem, a fluorescent polymer (PLGA marked with fluorescein from Polyscitech) was also tested. Accordingly to the supplier, this fluorescent polymer must be mixed with non-fluorescent PLGA, in a minimum ratio of 1:10. Therefore, this mixture was performed in a ratio of 1:4. The particles were then prepared by Nanoprecipitation, accordingly to the previous described method. However, results (data not shown) did not show the presence of any fluorescent particle. Therefore, as the polymer was not working, it could not be further explored for this purpose.

In what concerns the Large particles, these were, in a general way, internalized at higher percentages. However, it was observed that in multinucleated cells, cells with 2 or 3 nuclei internalized at a larger scale than cells with more than 8 nuclei. This led to the conclusion that as the cell is more mature towards osteoclasts phenotype, it has less capacity to internalize the particles. Further studies must be performed on this topic in order to understand this behavior.

4.4. Nanofibers

Considering the fact that the drug delivery system is aimed to be applied locally in a bone defect, in addition to the controlled delivery of the drug a support for the particle system must also be considered. In a way to circumvent such aspect, in this work it was also considered the preparation of nanofibers. Nanofibers can act as a scaffold, providing support for bone remodeling. Moreover, they act in the extracellular environment, therefore eliminating the disadvantageous variable of internalization, and their high surface area allows higher drug loadings [126, 159].

In order to test which was the best formulation to obtain nanofibers, different polymer concentrations and solvents were experimented (Figure 15). Figure 15-A represents nanofibers of 17.0% (wt/vol) PCL in acetone, a formulation optimized and used by another element of INEB, Juliana Dias, who kindly offered her solution in order to better understand which were the appearance of nanofibers and the behavior of the jet during the electrospinning process. Her result shows a randomly organized fiber mat, which arises from a stationary collector. However, Figure 15-A only serves as a term of comparison (or a positive control) to the other nanofibers' formulations. Figure 15-B and 17-C correspond to 10% and 13% (wt/vol) of PCL in 1:0 of DCM:DMF, respectively. As it is observed, instead of obtaining fibers, it was only obtained beads. This may be associated to a jet instability referred as droplet-break up, that usually occurs in more diluted solutions. This type of instability, instead of electrospinning, usually leads to electrospraying, which is described as the process in which electrostatic forces are used to form droplets, instead of fibers [122]. In some situations, this instability cannot be completely suppressed, leading to beads-on-string morphologies in electrospun fibers, which is the morphology present in the fibers of Figure 15-D, that corresponds to 15.0% (wt/vol) of PCL in 1:0 of DCM:DMF. However, when the formulations of 10.0%, 13.0% and 15.0% (wt/vol) of PCL in 1:0 of DCM:DMF are compared between each other, it can be observed that as the polymer concentration is higher, the presence of beads is lower and the result passes from beads to fibers with beads. In fact, polymer concentration is of major importance, as it determines the spinnability of a solution by influencing both the viscosity and surface tension of the solution [120, 126]. If the solution is too diluted, fibers will tend to break and form droplets before reaching the collector; on the other hand, if it is too concentrated, then the viscosity will be so high that it becomes impossible to form fibers [126]. Therefore, it must be reached a balance between too high and too low concentrations, in order to obtain a solution neither too viscous nor too diluted. The results show that the percentages of 10.0% and 13.0% (wt/vol) of PCL are too low to obtain any kind of fibers, while 15.0% is almost ideal, as it is observed the presence of fibers, although with beads. An experiment with higher concentrations probably would result in fibers without beads. However, the solution of 15.0% (wt/vol) of PCL was already too viscous, leading to some solidification of the fibers in the needle. Therefore, other parameters were modified in order to observe the influence of other factors that could result in nanofibers.

In what concerns Figure 15-E and F, these correspond to results from the same sample with 10.0% (wt/vol) of PCL in 4:1 of DCM:DMF. In Figure 15-E it is observed the presence of clusters of beads, which may be associated to the deposition of beads with electrically charged solvent, that will attract another beads and so on. However, in Figure 15-F the results show the presence of fibers with some beads. The difference present in distinct regions of the same sample may be associated to some kind of instability during the procedure. As humidity, temperature, air density and air viscosity may influence the electrospinning procedure [123], some variability on these parameters in a certain period of the procedure may have caused this difference on the samples. The addition of DMF intended to augment the viscosity of the solution, as well as its conductivity [126, 139]. Conductivity will essentially affect the nanofibers' diameter, which decreases with the solution's conductivity augmentation [126] and viscosity will affect the parameters as previously described. When comparing Figure 15-B and F, which in their formulations only differ in the solvent type, it is observed that Figure 15-F has an aspect more similar to fibers than Figure 15-B. This may be associated to the solution's viscosity, which was increased with the addition of the DMF solvent.

Therefore, by analyzing all the parameters, it was conclude that by augmenting the polymer's concentration and the content in DMF, the possibility of obtaining fibers is higher. However, the experiments could not be followed due to the degradation of the polymer, which may have also been the reason why any of the formulations resulted in the formation of nanofibers.

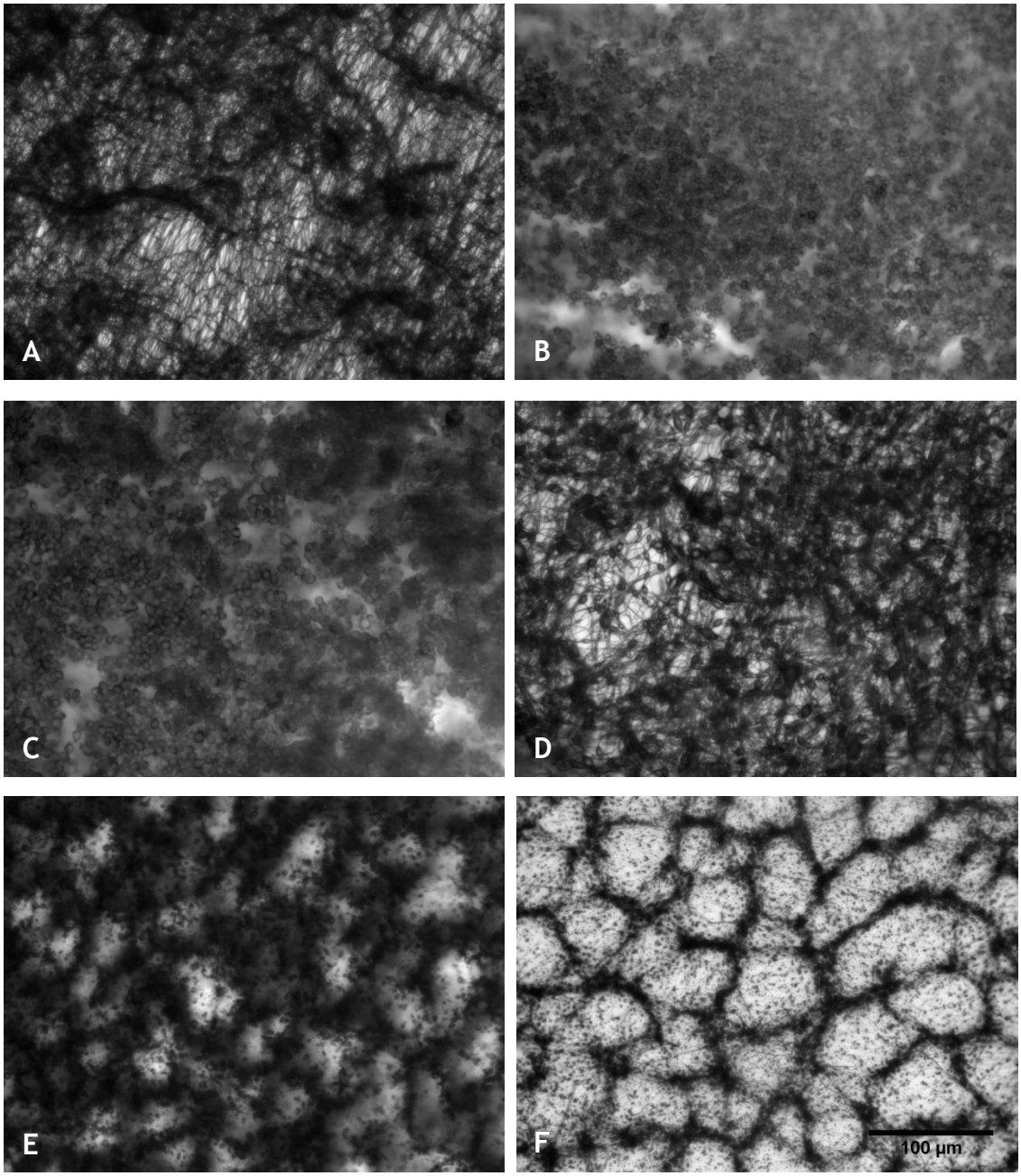

Figure 15. Nanofibers produced by electrospinning at 1Kv/cm, with a distance of 14 cm between the spinneret and the collector. (A) Results from the solution of 17.0% (wt/vol) of PCL in acetone. (B) Results from the solution of 10.0% (wt/vol) of PCL in 1:0 of DCM:DMF. (C) Results from the solution of 13.0% (wt/vol) of PCL in 1:0 of DCM:DMF. (D) Results from the solution of 15.0% (wt/vol) of PCL in 1:0 of DCM:DMF. (E) and (F) Results from the solution of 10.0% (wt/vol) of PCL in 4:1 of DCM:DMF. All images were taken in an Inverted Fluorescence Microscope. Scale bar present in Figure (F).

CHAPTER 5

Conclusion and Future Perspectives

In the present study, it was aimed the formulation and optimization of particles and nanofibers-based drug delivery systems for the local delivery of an Y1 receptor antagonist, BIBP3226. Two main considerations needed to be taken into account: as BIBP3226 is an hydrophobic drug, hydrophobic polymers should be used to prepare the delivery systems and, as Y1 receptor is transmembranar, the drug release must occur in the extracellular space.

Therefore, during these 6 months, PLGA and PCL particles were successfully produced. Due to PCL degradation, PLGA was chosen to procced with the project. Two methods (Salting-out and Nanoprecipitation) were optimized for the attainment of PLGA particles with sizes comprised between 100 nm and 200 nm, 400 nm and 500 nm, 800 nm and 1000 nm. After obtaining particles with sizes within these ranges, their cytotoxicity was studied and internalization rates were assessed in Bone Marrow derived cells. Any of the differently sized particles has shown cytotoxicity, as cells remained viable and with high levels of metabolic activity. In what concerns their internalization, results have shown higher rates of internalization for the particles within the range from 800 nm to 1000 nm, when compared to particles with sizes from 400 nm to 500 nm. In what concerns particles with sizes from 100 nm to 200 nm, results were inconclusive. Besides these studies, it was also assessed if a variation on the volumes used in the preparation of particles by the Salting-out method would influence the particles size and drug loading efficiency. Results have shown that size is not influenced, but in what concerns drug loading efficiency, it may have influence. However, further experiments should be performed in order to confirm the results. In what concerns nanofibers, as the polymer was degraded, conclusions could not be taken for the tested formulations.

During my Master thesis, I was able to attain experience in particles preparation by two different methods, nanofibers preparation by electrospinning, cell culture techniques, Confocal and Inverted Fluorescence Microscopy and Image Flow Cytometry. However, due to time restrictions and difficulties with equipment and materials, some limitations were imposed. Namely the number of replicas in some experiments was too low, the evaluation of results could not be performed as initially expected and experiments could not be carried on.

Therefore, some future improvements are here proposed in order to confirm the obtained conclusions.

Filtration was performed as a purification method in the Nanoprecipitation method, revealing good results for particles' size before Freeze-Drying. This purification procedure must be studied in what concerns mass losses and possibilities of introducing some kind of cryoprotectant or surfactant, in order to raise the particles stability during Freeze-Drying. By performing this study, if filtration shows good results for the aforementioned parameters, centrifugation can be substituted by this procedure, as filtration is more efficient in the elimination of aggregates and coalesced particles.

In what concerns the internalization studies, these must be performed using a polymer marked with fluorescence, as it not only eliminates the release kinetics present in Coumarin-6 loaded particles, but also allows the evaluation of results by Image Flow Cytometry. Besides this method, results should be assessed by FACS or by measuring the total fluorescence of the image, which was not possible due to the high fluorescence of Coumarin-6. Regarding the cells, it must be assessed if the cells present in culture are osteoclasts, by using the same markers that Francisco Conceição has used (TRAP staining, TRAP release quantification RT-PCR for genes that typify the osteoclast lineage, like cathepsin K, osteoclast-associated receptor and calcitonin receptor).

As nanofibers could not be produced due to the polymer degradation, the procedure should be repeated with new PCL in order to evaluate the tested conditions and obtain nanofibers.

As general future improvements, more replicas should be performed in every experiment in order to confirm the obtained results. Consequently, the optimized particles and nanofibers should be tested in what concerns their release kinetics and loading capacities. By optimizing these two parameters, the two delivery systems should be tested in the delivery of BIBP3226 at bone marrow derived cells and, after assessing these results, studies should be performed *in vivo*.

References

1. Lee, N.J. and H. Herzog, *NPY regulation of bone remodelling*. Neuropeptides, 2009. **43**(6): p. 457-63.
2. Del Fattore, A., A. Teti, and N. Rucci, *Bone cells and the mechanisms of bone remodelling*. Front Biosci (Elite Ed), 2012. **4**: p. 2302-21.
3. Seeley, R.D., T.D. Stephens, and P. Tate, *Anatomia & fisiologia*. 1993: Sorbona.
4. Gaalen, S.v., et al., *Chapter 19 - Tissue engineering of bone*, in *Tissue Engineering*, C.v. Blitterswijk, et al., Editors. 2008, Academic Press: Burlington. p. 559-610.
5. Currey, J.D., *Bones: Structure and Mechanics*. 2013: Princeton University Press. 456.
6. Feng, W., et al., *Osteoclastogenesis and osteoimmunology*. Front Biosci (Landmark Ed), 2014. **19**: p. 758-67.
7. Giganti, M.G., et al., *Fracture healing: from basic science to role of nutrition*. Front Biosci (Landmark Ed), 2014. **19**: p. 1162-75.
8. Dimitriou, R., et al., *Bone regeneration: current concepts and future directions*. BMC Med, 2011. **9**: p. 66.
9. Shi, Y.C. and P.A. Baldock, *Central and peripheral mechanisms of the NPY system in the regulation of bone and adipose tissue*. Bone, 2012. **50**(2): p. 430-6.
10. Gehlert, D.R., *Introduction to the reviews on neuropeptide Y*. Neuropeptides, 2004. **38**(4): p. 135-40.
11. Blomqvist, A.G. and H. Herzog, *Y-receptor subtypes--how many more?* Trends Neurosci, 1997. **20**(7): p. 294-8.
12. Khor, E.C. and P. Baldock, *The NPY system and its neural and neuroendocrine regulation of bone*. Curr Osteoporos Rep, 2012. **10**(2): p. 160-8.
13. Tatemoto, K., *Neuropeptide Y: complete amino acid sequence of the brain peptide*. Proc Natl Acad Sci U S A, 1982. **79**(18): p. 5485-9.
14. Lin, S., D. Boey, and H. Herzog, *NPY and Y receptors: lessons from transgenic and knockout models*. Neuropeptides, 2004. **38**(4): p. 189-200.
15. Nunes, A.F., et al., *Neuropeptide Y expression and function during osteoblast differentiation--insights from transthyretin knockout mice*. FEBS J, 2010. **277**(1): p. 263-75.
16. Parker, R.M. and H. Herzog, *Regional distribution of Y-receptor subtype mRNAs in rat brain*. Eur J Neurosci, 1999. **11**(4): p. 1431-48.
17. Sisask, G., et al., *The development of autonomic innervation in bone and joints of the rat*. J Auton Nerv Syst, 1996. **59**(1-2): p. 27-33.
18. Baldock, P.A., et al., *Novel role of Y1 receptors in the coordinated regulation of bone and energy homeostasis*. J Biol Chem, 2007. **282**(26): p. 19092-102.
19. Baldock, P.A., et al., *Hypothalamic Y2 receptors regulate bone formation*. J Clin Invest, 2002. **109**(7): p. 915-21.
20. Allison, S.J., P.A. Baldock, and H. Herzog, *The control of bone remodeling by neuropeptide Y receptors*. Peptides, 2007. **28**(2): p. 320-5.
21. Lundberg, P., et al., *Greater bone formation of Y2 knockout mice is associated with increased osteoprogenitor numbers and altered Y1 receptor expression*. J Biol Chem, 2007. **282**(26): p. 19082-91.
22. Sousa, D.M., et al., *Neuropeptide Y Y1 receptor antagonism increases bone mass in mice*. Bone, 2012. **51**(1): p. 8-16.
23. Sainsbury, A., et al., *Synergistic effects of Y2 and Y4 receptors on adiposity and bone mass revealed in double knockout mice*. Mol Cell Biol, 2003. **23**(15): p. 5225-33.
24. Lee, N.J., et al., *Osteoblast specific Y1 receptor deletion enhances bone mass*. Bone, 2011. **48**(3): p. 461-7.
25. Desai, S.J., et al., *Neuropeptide Y attenuates anxiety- and depression-like effects of cholecystokinin-4 in mice*. Neuroscience, 2014. **277**: p. 818-30.
26. Kask, A., L. Rago, and J. Harro, *Alpha-helical CRF(9-41) prevents anxiogenic-like effect of NPY Y1 receptor antagonist BIBP3226 in rats*. Neuroreport, 1997. **8**(16): p. 3645-7.

27. Kask, A., L. Rago, and J. Harro, *NPY Y1 receptors in the dorsal periaqueductal gray matter regulate anxiety in the social interaction test*. Neuroreport, 1998. **9**(12): p. 2713-6.
28. Kask, A., L. Rägo, and J. Harro, *Anxiogenic-like effect of the neuropeptide Y Y1 receptor antagonist BIBP3226: antagonism with diazepam*. European Journal of Pharmacology, 1996. **317**(2–3): p. R3-R4.
29. Kask, A., et al., *Neuropeptide Y Y(5) receptor antagonist CGP71683A: the effects on food intake and anxiety-related behavior in the rat*. Eur J Pharmacol, 2001. **414**(2-3): p. 215-24.
30. Smialowska, M., et al., *The effect of intrahippocampal injection of group II and III metobotropic glutamate receptor agonists on anxiety; the role of neuropeptide Y*. Neuropsychopharmacology, 2007. **32**(6): p. 1242-50.
31. Trent, N.L. and J.L. Menard, *Infusions of neuropeptide Y into the lateral septum reduce anxiety-related behaviors in the rat*. Pharmacol Biochem Behav, 2011. **99**(4): p. 580-90.
32. Daniels, A.J., et al., *Food intake inhibition and reduction in body weight gain in rats treated with GI264879A, a non-selective NPY-Y1 receptor antagonist*. Peptides, 2001. **22**(3): p. 483-91.
33. Hipskind, P.A., et al., *Potent and selective 1,2,3-trisubstituted indole NPY Y-1 antagonists*. J Med Chem, 1997. **40**(23): p. 3712-4.
34. Ida, T., et al., *Both corticotropin releasing factor and neuropeptide Y are involved in the effect of orexin (hypocretin) on the food intake in rats*. Neurosci Lett, 2000. **293**(2): p. 119-22.
35. Kanatani, A., et al., *The novel neuropeptide Y Y(1) receptor antagonist J-104870: a potent feeding suppressant with oral bioavailability*. Biochem Biophys Res Commun, 1999. **266**(1): p. 88-91.
36. Kask, A., L. Rago, and J. Harro, *Evidence for involvement of neuropeptide Y receptors in the regulation of food intake: studies with Y1-selective antagonist BIBP3226*. Br J Pharmacol, 1998. **124**(7): p. 1507-15.
37. Lecklin, A., et al., *Receptor subtypes Y1 and Y5 mediate neuropeptide Y induced feeding in the guinea-pig*. Br J Pharmacol, 2002. **135**(8): p. 2029-37.
38. Narnaware, Y.K., et al., *Regulation of food intake by neuropeptide Y in goldfish*. Am J Physiol Regul Integr Comp Physiol, 2000. **279**(3): p. R1025-34.
39. Polidori, C., et al., *Neuropeptide Y receptor(s) mediating feeding in the rat: characterization with antagonists*. Peptides, 2000. **21**(1): p. 29-35.
40. Wieland, H.A., et al., *Subtype selectivity of the novel nonpeptide neuropeptide Y Y1 receptor antagonist BIBO 3304 and its effect on feeding in rodents*. Br J Pharmacol, 1998. **125**(3): p. 549-55.
41. Gariboldi, M., et al., *Anticonvulsant properties of BIBP3226, a non-peptide selective antagonist at neuropeptide Y Y1 receptors*. Eur J Neurosci, 1998. **10**(2): p. 757-9.
42. Ghahramanian Golzar, M., et al., *NPY Receptors Blockade Prevents Anticonvulsant Action of Ghrelin in the Hippocampus of Rat*. Adv Pharm Bull, 2013. **3**(2): p. 265-71.
43. Redrobe, J.P., et al., *The neuropeptide Y (NPY) Y1 receptor subtype mediates NPY-induced antidepressant-like activity in the mouse forced swimming test*. Neuropsychopharmacology, 2002. **26**(5): p. 615-24.
44. Ishida, H., et al., *Infusion of neuropeptide Y into CA3 region of hippocampus produces antidepressant-like effect via Y1 receptor*. Hippocampus, 2007. **17**(4): p. 271-80.
45. Dimitrijevic, M., et al., *Effect of neuropeptide Y on inflammatory paw edema in the rat: involvement of peripheral NPY Y1 and Y5 receptors and interaction with dipeptidyl-peptidase IV (CD26)*. J Neuroimmunol, 2002. **129**(1-2): p. 35-42.
46. Kuphal, K.E., et al., *Y1 receptor knockout increases nociception and prevents the anti-allodynic actions of NPY*. Nutrition, 2008. **24**(9): p. 885-91.
47. Lach, G. and T.C. de Lima, *Role of NPY Y1 receptor on acquisition, consolidation and extinction on contextual fear conditioning: dissociation between anxiety, locomotion and non-emotional memory behavior*. Neurobiol Learn Mem, 2013. **103**: p. 26-33.
48. Jaaskelainen, A.E., et al., *Systemic treatment with neuropeptide Y receptor Y1-antagonist enhances atherosclerosis and stimulates IL-12 expression in ApoE deficient mice*. Neuropeptides, 2013. **47**(2): p. 67-73.

49. Doods, H.N., et al., *Pharmacological characterization of the selective nonpeptide neuropeptide Y Y1 receptor antagonist BIBP 3226.* J Pharmacol Exp Ther, 1995. **275**(1): p. 136-42.
50. Zhao, X.H., et al., *Renal and cardiovascular role of the neuropeptide Y Y1 receptor in ischaemic heart failure rats.* J Pharm Pharmacol, 1999. **51**(11): p. 1257-65.
51. Chen, S.H. and R.T. Cheung, *Intracerebroventricular injection of a neuropeptide Y-Y1 receptor agonist increases while BIBP3226, a Y1 antagonist, reduces the infarct volume following transient middle cerebral artery occlusion in rats.* Neuroscience, 2003. **116**(1): p. 119-26.
52. Bergdahl, A., et al., *Neuropeptide Y potentiates noradrenaline-induced contraction through the neuropeptide Y Y1 receptor.* Eur J Pharmacol, 1996. **316**(1): p. 59-64.
53. Malmstrom, R.E., *Neuropeptide Y Y1 receptor mechanisms in sympathetic vascular control.* Acta Physiol Scand Suppl, 1997. **636**: p. 1-55.
54. Grundemar, L. and M. Ekelund, *Effects of the neuropeptide Y (NPY)-receptor antagonist BIBP3226 on vascular NPY-receptors with different ligand requirements.* Pharmacol Toxicol, 1996. **79**(5): p. 266-9.
55. Nilsson, T., L. Cantera, and L. Edvinsson, *Presence of neuropeptide Y Y1 receptor mediating vasoconstriction in human cerebral arteries.* Neurosci Lett, 1996. **204**(3): p. 145-8.
56. Dimitrov, E.L., et al., *Involvement of neuropeptide Y Y1 receptors in the regulation of neuroendocrine corticotropin-releasing hormone neuronal activity.* Endocrinology, 2007. **148**(8): p. 3666-73.
57. Li, Q., et al., *Neuropeptide Y protects cerebral cortical neurons by regulating microglial immune function.* Neural Regen Res, 2014. **9**(9): p. 959-67.
58. Dhillon, S.S., S. Gingerich, and D.D. Belsham, *Neuropeptide Y induces gonadotropin-releasing hormone gene expression directly and through conditioned medium from mHypoE-38 NPY neurons.* Regul Pept, 2009. **156**(1-3): p. 96-103.
59. Yu, L., S.C. An, and T. Lian, *[Involvement of hippocampal NMDA receptor and neuropeptide Y in depression induced by chronic unpredictable mild stress].* Sheng Li Xue Bao, 2010. **62**(1): p. 14-22.
60. Morton, K.D., M.J. McCloskey, and E.K. Potter, *Cardiorespiratory responses to intracerebroventricular injection of neuropeptide Y in anaesthetised dogs.* Regul Pept, 1999. **81**(1-3): p. 81-8.
61. McCloskey, M.J. and E.K. Potter, *Sympathetic and parasympathetic interaction in vascular and secretory control of salivary glands in anaesthetised dogs.* Auton Neurosci, 2000. **84**(1-2): p. 50-7.
62. Hassani, H., et al., *Attenuation of acute experimental colitis by preventing NPY Y1 receptor signaling.* Am J Physiol Gastrointest Liver Physiol, 2005. **288**(3): p. G550-6.
63. Malmstrom, R.E., et al., *In vivo characterization of the novel neuropeptide Y Y1 receptor antagonist H 409/22.* J Cardiovasc Pharmacol, 2000. **36**(4): p. 516-25.
64. Ishihara, A., et al., *Blockade of body weight gain and plasma corticosterone levels in Zucker fatty rats using an orally active neuropeptide Y Y1 antagonist.* Br J Pharmacol, 2002. **136**(3): p. 341-6.
65. Malmstrom, R.E. and J.M. Lundberg, *Effects of the neuropeptide YY1 receptor antagonist SR 120107A on sympathetic vascular control in pigs in vivo.* Naunyn Schmiedebergs Arch Pharmacol, 1996. **354**(5): p. 633-42.
66. Serradeil-Le Gal, C., et al., *Characterization of NPY receptors controlling lipolysis and leptin secretion in human adipocytes.* FEBS Lett, 2000. **475**(2): p. 150-6.
67. Dumont, Y., et al., *Potent and selective tools to investigate neuropeptide Y receptors in the central and peripheral nervous systems: BIB03304 (Y1) and CGP71683A (Y5).* Can J Physiol Pharmacol, 2000. **78**(2): p. 116-25.
68. Dumont, Y. and R. Quirion, *[(125)I]-GR231118: a high affinity radioligand to investigate neuropeptide Y Y(1) and Y(4) receptors.* Br J Pharmacol, 2000. **129**(1): p. 37-46.
69. Doods, H.N., et al., *BIBP 3226, the first selective neuropeptide Y1 receptor antagonist: a review of its pharmacological properties.* Regul Pept, 1996. **65**(1): p. 71-7.
70. Rudolf, K., et al., *The first highly potent and selective non-peptide neuropeptide Y Y1 receptor antagonist: BIBP3226.* Eur J Pharmacol, 1994. **271**(2-3): p. R11-3.
71. *Current Pharmaceutical Design*. 12 ed. Vol. 5. 1999: Bentham Science Publishers.

72. Schober, D.A., et al., *The neuropeptide Y Y1 antagonist, 1229U91, a potent agonist for the human pancreatic polypeptide-preferring (NPY Y4) receptor*. Peptides, 1998. **19**(3): p. 537-42.
73. Kanatani, A., et al., *A typical Y1 receptor regulates feeding behaviors: effects of a potent and selective Y1 antagonist, J-115814*. Mol Pharmacol, 2001. **59**(3): p. 501-5.
74. Sjodin, P., et al., *Re-evaluation of receptor-ligand interactions of the human neuropeptide Y receptor Y1: a site-directed mutagenesis study*. Biochem J, 2006. **393**(Pt 1): p. 161-9.
75. Serradeil-Le Gal, C., et al., *SR 120819A, an orally-active and selective neuropeptide Y Y1 receptor antagonist*. FEBS Lett, 1995. **362**(2): p. 192-6.
76. Bauer, T.W. and G.F. Muschler, *Bone graft materials. An overview of the basic science*. Clin Orthop Relat Res, 2000(371): p. 10-27.
77. St John, T.A., et al., *Physical and monetary costs associated with autogenous bone graft harvesting*. Am J Orthop (Belle Mead NJ), 2003. **32**(1): p. 18-23.
78. Giannoudis, P.V., H. Dinopoulos, and E. Tsiridis, *Bone substitutes: an update*. Injury, 2005. **36 Suppl 3**: p. S20-7.
79. Gittens, S.A., et al., *Designing proteins for bone targeting*. Adv Drug Deliv Rev, 2005. **57**(7): p. 1011-36.
80. Hirabayashi, H. and J. Fujisaki, *Bone-specific drug delivery systems: approaches via chemical modification of bone-seeking agents*. Clin Pharmacokinet, 2003. **42**(15): p. 1319-30.
81. Shuid, A.N., et al., *Drug delivery systems for prevention and treatment of osteoporotic fracture*. Curr Drug Targets, 2013. **14**(13): p. 1558-64.
82. Tautzenberger, A., A. Kovtun, and A. Ignatius, *Nanoparticles and their potential for application in bone*. Int J Nanomedicine, 2012. **7**: p. 4545-57.
83. Bose, S. and S. Tarafder, *Calcium phosphate ceramic systems in growth factor and drug delivery for bone tissue engineering: a review*. Acta Biomater, 2012. **8**(4): p. 1401-21.
84. des Rieux, A., et al., *Nanoparticles as potential oral delivery systems of proteins and vaccines: a mechanistic approach*. J Control Release, 2006. **116**(1): p. 1-27.
85. Xinluan, W., et al., *Systemic Drug Delivery Systems for Bone Tissue Regeneration- A Mini Review*. Curr Pharm Des, 2015.
86. Petros, R.A. and J.M. DeSimone, *Strategies in the design of nanoparticles for therapeutic applications*. Nat Rev Drug Discov, 2010. **9**(8): p. 615-27.
87. Yasmeen, S., et al., *Injectable scaffolds for bone regeneration*. Langmuir, 2014. **30**(43): p. 12977-85.
88. Xu, H.H., M.D. Weir, and C.G. Simon, *Injectable and strong nano-apatite scaffolds for cell/growth factor delivery and bone regeneration*. Dent Mater, 2008. **24**(9): p. 1212-22.
89. Anthony, M.L. and L.H. Meredith, *Nanoparticles for Drug Delivery*, in *Handbook of Nanoscience, Engineering, and Technology, Second Edition*. 2007, CRC Press. p. 30-1-30-28.
90. Torchilin, V. and M.M. Amiji, *Handbook of Materials for Nanomedicine*. 2010: Pan Stanford Publishing Pte. Ltd.
91. Vauthier, C. and K. Bouchemal, *Methods for the preparation and manufacture of polymeric nanoparticles*. Pharm Res, 2009. **26**(5): p. 1025-58.
92. Kumari, A., S.K. Yadav, and S.C. Yadav, *Biodegradable polymeric nanoparticles based drug delivery systems*. Colloids and Surfaces B: Biointerfaces, 2010. **75**(1): p. 1-18.
93. Leite, D.M., *Design of a Controlled Delivery System to Promote Osteogenesis*. 2012, Faculty of Engineering of University of Porto, Portugal.
94. Ulery, B.D., L.S. Nair, and C.T. Laurencin, *Biomedical Applications of Biodegradable Polymers*. J Polym Sci B Polym Phys, 2011. **49**(12): p. 832-864.
95. Makadia, H.K. and S.J. Siegel, *Poly Lactic-co-Glycolic Acid (PLGA) as Biodegradable Controlled Drug Delivery Carrier*. Polymers, 2011. **3**(3): p. 1377-1397.
96. Schrier, J.A. and P.P. DeLuca, *Recombinant human bone morphogenetic protein-2 binding and incorporation in PLGA microsphere delivery systems*. Pharm Dev Technol, 1999. **4**(4): p. 611-21.

97. Yilgor, P., et al., *Incorporation of a sequential BMP-2/BMP-7 delivery system into chitosan-based scaffolds for bone tissue engineering.* Biomaterials, 2009. **30**(21): p. 3551-9.
98. Wei, G., et al., *The enhancement of osteogenesis by nano-fibrous scaffolds incorporating rhBMP-7 nanospheres.* Biomaterials, 2007. **28**(12): p. 2087-96.
99. Park, J.S., et al., *PLGA microsphere construct coated with TGF-beta 3 loaded nanoparticles for neocartilage formation.* Biomacromolecules, 2008. **9**(8): p. 2162-9.
100. Pillai, R.R., et al., *Nafcillin-loaded PLGA nanoparticles for treatment of osteomyelitis.* Biomed Mater, 2008. **3**(3): p. 034114.
101. Otsuka, M., et al., *Therapeutic effect of in vivo sustained estradiol release from poly (lactide-co-glycolide) microspheres on bone mineral density of osteoporosis rats.* Biomed Mater Eng, 2002. **12**(2): p. 157-67.
102. Dawes, G.J., et al., *Effects of dexamethasone-loaded PLGA microspheres on human fetal osteoblasts.* J Biomater Appl, 2012. **27**(4): p. 477-83.
103. Zhang, Z., D.W. Grijpma, and J. Feijen, *Thermo-sensitive transition of monomethoxy poly(ethylene glycol)-block-poly(trimethylene carbonate) films to micellar-like nanoparticles.* J Control Release, 2006. **112**(1): p. 57-63.
104. Zhang, Z., *Biodegradable Block Copolymers Based On Trimethylene Carbonate, Lactides, And Poly(Ethylene Glycol)*. 2006, University of Twente.
105. Moghadam, B.Y., et al., *Role of nanoparticle surface functionality in the disruption of model cell membranes.* Langmuir, 2012. **28**(47): p. 16318-26.
106. Kettler, K., et al., *Cellular uptake of nanoparticles as determined by particle properties, experimental conditions, and cell type*. Environmental Toxicology and Chemistry, 2014. **33**(3): p. 481-492.
107. Sylvester, A., et al., *Nanoparticles for localized delivery of hyaluronan oligomers towards regenerative repair of elastic matrix.* Acta Biomater, 2013. **9**(12): p. 9292-302.
108. Sivaraman, B. and A. Ramamurthi, *Multifunctional nanoparticles for doxycycline delivery towards localized elastic matrix stabilization and regenerative repair.* Acta Biomater, 2013. **9**(5): p. 6511-25.
109. Wang, S.H., et al., *Size-dependent endocytosis of gold nanoparticles studied by three-dimensional mapping of plasmonic scattering images.* J Nanobiotechnology, 2010. **8**: p. 33.
110. Osaki, F., et al., *A quantum dot conjugated sugar ball and its cellular uptake. On the size effects of endocytosis in the subviral region.* J Am Chem Soc, 2004. **126**(21): p. 6520-1.
111. Chithrani, B.D., A.A. Ghazani, and W.C. Chan, *Determining the size and shape dependence of gold nanoparticle uptake into mammalian cells.* Nano Lett, 2006. **6**(4): p. 662-8.
112. Chithrani, B.D. and W.C. Chan, *Elucidating the mechanism of cellular uptake and removal of protein-coated gold nanoparticles of different sizes and shapes.* Nano Lett, 2007. **7**(6): p. 1542-50.
113. Panyam, J. and V. Labhasetwar, *Biodegradable nanoparticles for drug and gene delivery to cells and tissue.* Adv Drug Deliv Rev, 2003. **55**(3): p. 329-47.
114. Gratton, S.E., et al., *The effect of particle design on cellular internalization pathways.* Proc Natl Acad Sci U S A, 2008. **105**(33): p. 11613-8.
115. Clift, M.J., et al., *The impact of different nanoparticle surface chemistry and size on uptake and toxicity in a murine macrophage cell line.* Toxicol Appl Pharmacol, 2008. **232**(3): p. 418-27.
116. Champion, J.A. and S. Mitragotri, *Role of target geometry in phagocytosis.* Proc Natl Acad Sci U S A, 2006. **103**(13): p. 4930-4.
117. Patil, S., et al., *Protein adsorption and cellular uptake of cerium oxide nanoparticles as a function of zeta potential.* Biomaterials, 2007. **28**(31): p. 4600-7.
118. Raz, A., et al., *Biochemical, morphological, and ultrastructural studies on the uptake of liposomes by murine macrophages.* Cancer Res, 1981. **41**(2): p. 487-94.
119. He, C., et al., *Effects of particle size and surface charge on cellular uptake and biodistribution of polymeric nanoparticles.* Biomaterials, 2010. **31**(13): p. 3657-66.
120. Chew, S.Y., et al., *The role of electrospinning in the emerging field of nanomedicine.* Curr Pharm Des, 2006. **12**(36): p. 4751-70.

121. Agarwal, S., J.H. Wendorff, and A. Greiner, *Use of electrospinning technique for biomedical applications*. Polymer, 2008. **49**(26): p. 5603-5621.
122. Rutledge, G.C. and S.V. Fridrikh, *Formation of fibers by electrospinning*. Adv Drug Deliv Rev, 2007. **59**(14): p. 1384-91.
123. Pham, Q.P., U. Sharma, and A.G. Mikos, *Electrospinning of polymeric nanofibers for tissue engineering applications: a review*. Tissue Eng, 2006. **12**(5): p. 1197-211.
124. Liu, H., et al., *Electrospinning of Nanofibers for Tissue Engineering Applications*. Journal of Nanomaterials, 2013. **2013**: p. 11.
125. Kriegel, C., et al., *Fabrication, functionalization, and application of electrospun biopolymer nanofibers*. Crit Rev Food Sci Nutr, 2008. **48**(8): p. 775-97.
126. Sill, T.J. and H.A. von Recum, *Electrospinning: applications in drug delivery and tissue engineering*. Biomaterials, 2008. **29**(13): p. 1989-2006.
127. Meinel, A.J., et al., *Electrospun matrices for localized drug delivery: current technologies and selected biomedical applications*. Eur J Pharm Biopharm, 2012. **81**(1): p. 1-13.
128. Karageorgiou, V. and D. Kaplan, *Porosity of 3D biomaterial scaffolds and osteogenesis*. Biomaterials, 2005. **26**(27): p. 5474-91.
129. Shin, M., H. Yoshimoto, and J.P. Vacanti, *In vivo bone tissue engineering using mesenchymal stem cells on a novel electrospun nanofibrous scaffold*. Tissue Eng, 2004. **10**(1-2): p. 33-41.
130. Ruckh, T.T., et al., *Osteogenic differentiation of bone marrow stromal cells on poly(epsilon-caprolactone) nanofiber scaffolds*. Acta Biomater, 2010. **6**(8): p. 2949-59.
131. Yoshimoto, H., et al., *A biodegradable nanofiber scaffold by electrospinning and its potential for bone tissue engineering*. Biomaterials, 2003. **24**(12): p. 2077-82.
132. Tuzlakoglu, K., et al., *Nano- and micro-fiber combined scaffolds: a new architecture for bone tissue engineering*. J Mater Sci Mater Med, 2005. **16**(12): p. 1099-104.
133. Pham, Q.P., U. Sharma, and A.G. Mikos, *Electrospun poly(epsilon-caprolactone) microfiber and multilayer nanofiber/microfiber scaffolds: characterization of scaffolds and measurement of cellular infiltration*. Biomacromolecules, 2006. **7**(10): p. 2796-805.
134. Piskin, E., et al., *In vivo performance of simvastatin-loaded electrospun spiral-wound polycaprolactone scaffolds in reconstruction of cranial bone defects in the rat model*. J Biomed Mater Res A, 2009. **90**(4): p. 1137-51.
135. Yoshimoto, H., et al., *A biodegradable nanofiber scaffold by electrospinning and its potential for bone tissue engineering*. Biomaterials, 2003. **24**(12): p. 2077-2082.
136. Cheng, J., et al., *Formulation of functionalized PLGA-PEG nanoparticles for in vivo targeted drug delivery*. Biomaterials, 2007. **28**(5): p. 869-76.
137. Chang, J., et al., *Transferrin adsorption onto PLGA nanoparticles governs their interaction with biological systems from blood circulation to brain cancer cells*. Pharm Res, 2012. **29**(6): p. 1495-505.
138. Zhang, Z., D.W. Grijpma, and J. Feijen, *Poly(trimethylene carbonate) and monomethoxy poly(ethylene glycol)-block-poly(trimethylene carbonate) nanoparticles for the controlled release of dexamethasone*. J Control Release, 2006. **111**(3): p. 263-70.
139. Pires, L.R., et al., *Ibuprofen-loaded poly(trimethylene carbonate-co-epsilon-caprolactone) electrospun fibres for nerve regeneration*. J Tissue Eng Regen Med, 2013.
140. R., C.E.A., *Synthesis of poly(dl-lactide-co-glycolide) Nanoparticles with entrapped magnetite*. 2005, Faculty of the Louisiana State University and Agricultural and Mechanical College.
141. Galindo-Rodriguez, S., et al., *Physicochemical parameters associated with nanoparticle formation in the salting-out, emulsification-diffusion, and nanoprecipitation methods*. Pharm Res, 2004. **21**(8): p. 1428-39.
142. Sepassi, S., et al., *Effect of polymer molecular weight on the production of drug nanoparticles*. J Pharm Sci, 2007. **96**(10): p. 2655-66.
143. Budhian, A., S.J. Siegel, and K.I. Winey, *Haloperidol-loaded PLGA nanoparticles: systematic study of particle size and drug content*. Int J Pharm, 2007. **336**(2): p. 367-75.

144. Galindo-Rodríguez, S.A., et al., *Comparative scale-up of three methods for producing ibuprofen-loaded nanoparticles.* European Journal of Pharmaceutical Sciences, 2005. **25**(4–5): p. 357-367.
145. Konan, Y.N., R. Gurny, and E. Allemann, *Preparation and characterization of sterile and freeze-dried sub-200 nm nanoparticles.* Int J Pharm, 2002. **233**(1-2): p. 239-52.
146. Song, X., et al., *PLGA nanoparticles simultaneously loaded with vincristine sulfate and verapamil hydrochloride: systematic study of particle size and drug entrapment efficiency.* Int J Pharm, 2008. **350**(1-2): p. 320-9.
147. Sahoo, S.K., et al., *Residual polyvinyl alcohol associated with poly (D,L-lactide-co-glycolide) nanoparticles affects their physical properties and cellular uptake.* J Control Release, 2002. **82**(1): p. 105-14.
148. Zambaux, M.F., et al., *Influence of experimental parameters on the characteristics of poly(lactic acid) nanoparticles prepared by a double emulsion method.* J Control Release, 1998. **50**(1-3): p. 31-40.
149. Rahman, Z., et al., *Understanding the quality of protein loaded PLGA nanoparticles variability by Plackett–Burman design.* International Journal of Pharmaceutics, 2010. **389**(1–2): p. 186-194.
150. Hueper, W.C., *Carcinogenic studies on water-soluble and insoluble macromolecules.* AMA Arch Pathol, 1959. **67**(6): p. 589-617.
151. Saez, A., et al., *Freeze-drying of polycaprolactone and poly(d,l-lactic-glycolic) nanoparticles induce minor particle size changes affecting the oral pharmacokinetics of loaded drugs.* European Journal of Pharmaceutics and Biopharmaceutics, 2000. **50**(3): p. 379-387.
152. *International Standards Organization. ISO 10993-5. Biological evaluation of medical devices. Tests for in vitro cytotoxicity. Geneva: International Standards Organization, 2009.*
153. Rivolta, I., et al., *Cellular uptake of coumarin-6 as a model drug loaded in solid lipid nanoparticles.* J Physiol Pharmacol, 2011. **62**(1): p. 45-53.
154. Pan, Y., et al., *Size-dependent cytotoxicity of gold nanoparticles.* Small, 2007. **3**(11): p. 1941-9.
155. Kruth, H.S., et al., *Characterization of patocytosis: endocytosis into macrophage surface-connected compartments.* European Journal of Cell Biology, 1999. **78**(2): p. 91-99.
156. Win, K.Y. and S.S. Feng, *Effects of particle size and surface coating on cellular uptake of polymeric nanoparticles for oral delivery of anticancer drugs.* Biomaterials, 2005. **26**(15): p. 2713-22.
157. Cody, J.J., et al., *A simplified method for the generation of human osteoclasts in vitro.* International Journal of Biochemistry and Molecular Biology, 2011. **2**(2): p. 183-189.
158. van Furth, R., *Cells of the Mononuclear Phagocyte System*, in *Mononuclear Phagocytes*, R. van Furth, Editor. 1980, Springer Netherlands. p. 1-40.
159. Bhardwaj, N. and S.C. Kundu, *Electrospinning: a fascinating fiber fabrication technique.* Biotechnol Adv, 2010. **28**(3): p. 325-47.